UNIVERSIDAD DE LAS AMÉRICAS PUEBLA

School of Engineering

Department of Industrial and Mechanical Engineering

Comparison of the performance and emissions of gasoline and E10 in an internal combustion engine using Computational Fluid Dynamics simulation

Thesis submitted by the student to complete the requirements of the Honors Program

Ramón Alberto García Mena

168357

Mechanical Engineering

Thesis director: Dr. Rafael Carrera Espinoza

Thesis co-director: Dr. Pablo Moreno Garibaldi

San Andrés Cholula, Puebla. **Spring 2024**

Sheet of signatures

Thesis submitted by the student to complete the requirements of the Honors Program, Ramón Alberto García Mena, 168357

Director of Thesis

_____

Dr. Rafael Carrera Espinoza

Co-director of Thesis

_____

Dr. Pablo Moreno Garibaldi

President of the Thesis

_____

Dr. Christian Lagarza Cortés

Secretary of the Thesis

_____

Dr. Melvyn Álvarez Vera

Agradecimientos

Le quiero dar las gracias a mi familia, a mi mamá, a mi papá y a mi hermano por siempre apoyarme y haberme acompañado en esta etapa de mi vida; pero sobre todo a mi papá, por enseñarme tanto de coches y por creer en mí cuando ni siquiera yo lo hice.

Index

Index of figures

Abstract

In recent years, the use of biofuels has gained special attention from engineers, and car manufacturers as a way to reduce pollution and damage to the environment without discarding the internal combustion engine completely. In this thesis work, we compared the performance and exhaust emissions of a spark-ignition engine using gasoline and ethanol blends through Computational Fluid Dynamics simulation in Ansys Forte.

For this, the piston of the chosen engine was scanned and modeled in a simplified way for the simulation, as well as the head and liner geometries. Then, a volume was extracted from these geometries and a mesh was made. Then, after applying all the settings two simulations were performed, one with gasoline and another one with E10 from 1000 to 6000 RPM with increments of 500 RPM.

Through the simulations, it was determined that power output, torque, Indicated Mean Effective Pressure, and thermal efficiency were lower with E10 compared to gasoline. However, the specific fuel consumption was greater by 5.45% on average. Also, the better combustion offered by E10 contributed to the reduction in emissions of carbon monoxide (CO), carbon dioxide (CO_2), and nitrogen oxides (NO_x) by 5% to 6% on average. For unburnt hydrocarbons (UHC), the average reduction was 18.92% from 2000 to 6000 RPM.

From this research, it was concluded that despite the lower performance offered by E10 and higher fuel consumption, this fuel is adequate for reducing emissions in the future.

Keywords: gasoline, E10, engine, compression ratio, air/fuel ratio, piston, calorific value, thermal efficiency, power, fuel consumption, emissions

Introduction

The internal combustion engine was born at the end of the nineteenth century and developed by Nikolaus Otto, a German engineer. This type of engine gave birth to the first car in 1886, invented by Carl Benz. The internal combustion engine's operating principle is simple, air mixed with gasoline enters the cylinder, this mixture is compressed by a piston, later ignited by a spark plug, and finally exits as burnt gas. The explosion inside the cylinder is what ultimately powers the car.

Before fuel injection, mixture formation was achieved with carburetors. These devices mixed the entering air with the gasoline, this mixture was then regulated with a throttle valve to the cylinder. This type of mixture formation was used in most production vehicles up to the 1990s due to its lower cost, but nowadays, almost all cars if not all, use direct injection (Dietsche, 2015, p. 59). With injectors, fuel is sprayed directly within the cylinder allowing for lower fuel consumption and emissions, but at a higher cost for the car due to more electronic components being used (Dietsche, 2015, p. 50). The constant innovation for combustion gave rise to different engines and fuels. In 1892, Rudolf Diesel was issued a patent for the diesel engine (Dietsche, Kuhlgatz, 2015, p. 5). This type of engine is characterized by igniting the fuel by compression and not ignition like in the gasoline engine.

In the beginning of automotive development, there were steam, electric, and even gas engines; in the end, the one that prevailed was the internal combustion engine, whether diesel or gasoline. Why? Because refining oil into gasoline or diesel was cheaper than electricity at

the time. Also, no one thought about the dire long-term environmental consequences of burning fossil fuels.

Environmental problems all around the world are caused primarily due to human activities and have triggered a series of events that jeopardize our health and in the worst cases, global events that could even wipe out species. Such events are air pollution, which according to the World Health Organization (WHO) causes an estimated 4.2 million deaths globally per year (WHO, 2022); global warming and climate change, responsible for recent events like the flooding in Europe in 2021 (Fountain, 2021), wildfires in Australia during 2019 and 2020 (Phillips, 2020) and in California in 2021 (Fountain, 2021). What all of these problems have in common is their cause, the burning of fossil fuels.

Burning fossil fuels increases the quantity of greenhouse gas in the atmosphere, this traps heat and prevents it from escaping, thus raising the Earth's average temperature (National Aeronautics and Space Administration, 2022, par. 7). Based on global emissions from 2010, the Intergovernmental Panel on Climate Change (as cited on the United States Environmental Protection Agency, 2022) determined that greenhouse gas emissions from the industrial and transportation sectors alone accounted for 21 and 14% respectively, of the total. In both sectors, the automobile industry has a serious impact because emissions come from extracting the raw materials needed for and building the car. Furthermore, if these cars use internal combustion engines, even more emissions are released when they finally hit the road.

The problem of internal combustion engines is the pollution emitted after burning gasoline. Although automotive technology is advancing daily and environmental legislation

is becoming stricter, this is not enough to curb or at least counteract the emissions produced by the increasing number of automobiles.

As a response, several car manufacturers have committed to sustainability and started to pave the way for a net-zero carbon emissions target. Some examples include the Volkswagen Group (comprised of Volkswagen, Volkswagen Commercial Vehicles, Seat, Cupra, ŠKODA, Audi, Lamborghini, Bentley, Ducati, and Porsche) with its NEW AUTO strategy (Volkswagen AG, 2022), Honda, Tesla, and General Motors with its carbon-neutral plan for 2040 (General Motors Corporate Newsroom, 2021), among others. Even the Formula One World Championship has made efforts for sustainability, beginning in 2014 with the introduction of turbo-hybrid power units and a future commitment to fully sustainable fuels by 2025 (Formula One World Championship Limited, 2021).

That is why alternative forms of transportation have been proposed for several years. One of them, and perhaps the most popular today, are electric and hybrid vehicles. These pollute much less than a car with an internal combustion engine, but they are not perfect. Materials such as graphite, cobalt, lithium, manganese, and nickel (Backhaus, 2021, p. 1) are needed for the construction of these batteries, materials that if they are set free in the environment are dangerous for life. Materials or resources which, like gasoline, are finite.

Another of these different forms of transportation is more related to the type of fuel used. The use of fuels that can be renewed, as opposed to gasoline, is considered an option. These fuels are known as alternatives and range from biofuels, to the more recent synthetic fuels. Biofuels have sparked interest in the scientific community and the automotive industry

because they are cleaner than conventional gasoline or diesel, yet at a higher amount of fuel consumption.

All biofuels, liquid or solid, come from biomass, which makes up every living organism on Earth; thus, making it a renewable source. There are many types of biofuels, and some of them are ethanol and biodiesel. Ethanol is produced by the fermentation of sugars in plants like corn or sugarcane (Nunez, 2019, par. 5). Biodiesel, on the other hand, is produced by combining vegetable oils, animal fats, or recycled cooking grease with ethanol (Office of Energy Efficiency and Renewable Energy, par. 9-10).

Some of the most commonly used biofuels in the world are mixtures of gasoline and ethanol or ethanol-blended fuels. E10 is a biofuel made of 10% ethanol and 90% gasoline by volume, it is distributed throughout the United States (Nunez, 2019, par. 5) and in countries like Brazil, for example, higher ethanol blends starting from E20 are used (Belincanta, Alchorne, Teixeira da Silva, 2016, p. 1092). In motorsport, the Formula One championship has implemented mandatory use of E10 biofuel for all competitors in their technical regulations from the 2022 season onwards (*Fédération Internationale de l'Automobile*, 2022, p. 127).

Biofuels are relevant due to the raw materials needed for production and their emissions-reduction potential. Theoretically, using biofuels instead of regular gasoline has a lower environmental impact due to their lower content of pollutants (The Royal Society, 2008, p. 5) such as carbon dioxide (CO_2) carbon monoxide (CO), hydrocarbons (HC), among others. Nonetheless, its use can produce ozone precursors, aldehydes, and nitrogen oxides (NO_x) (The Royal Society, 2008, p. 32). Aldehydes (González *et al.*, 2018, p. 10, 12 &

Mohamad, Szepesi, & Bollo 2018, p. 30) are produced after ethanol combustion, and NO_x is produced due to a leaning effect (more air than gasoline) ethanol has on gasoline (González *et al.*, 2018, p. 6).

The problem with aldehydes and NO_x is the health risks they pose. Aldehydes are highly reactive and can modify DNA and proteins (Sinharoy, McAllister, Vasu, and Gross, 2019, p. 36), meaning that exposure to this chemical can increase the risk of cancer development and cardiovascular disease (Sinharoy *et al* 2019, p. 35 – 36).

Concerning NO_x, one of them is nitrogen dioxide (NO_2), which reacts with the sunlight and forms ozone and smog in the air (Agency for Toxic Substances and Disease Registry, 2014, par. 6). Low exposure levels of NO_x can irritate the eyes, nose, throat, lungs, and can produce sensations of nausea. High levels of exposure, however, can cause rapid burning, spasms, swelling of tissues in the respiratory systems, and ultimately, death (ATSDR, 2014, par. 14).

Because of the reasons mentioned earlier, the safety of using ethanol-gasoline blends regarding their emissions must be verified. In this work, the emissions-reduction potential of E10 when compared to gasoline will be validated through simulation, specifically, Computational Fluid Dynamics.

Justification

As a mechanical engineering student and soon-to-be bachelor, my main drive is my passion for cars, specifically, internal combustion engines. After graduation, I will dedicate myself to the design and perfection of the internal combustion engine. With this research work, I

will gain very valuable experience and knowledge that will help me strive towards that goal. The situations that justify the research done here are the following:

The first and most important is that the knowledge acquired during this work can be used in the future by other researchers on the same topic, in the same way, that this work builds on previous research and results. The second is that the technique known as Computational Fluid Dynamics (CFD) will be used to validate those results. Very briefly, CFD is a set of algorithms and numerical methods used for describing the movement of fluids, as well as its thermodynamics and heat transfer. Although most of the work that serves as a theoretical foundation was done in real life in a laboratory, what will be done in this work serves as a validation for what others did experimentally.

The third is that the data obtained will aid in a decision-making process that ultimately leads to an intervention; an intervention consisting of the large-scale implementation and use of biofuels. The last is that the research is related to an important aspect to solve, with the pollution by automobiles being the problem and the use of biofuels a possible solution, and the viability of this solution will be examined here.

Objectives

Main objective

Obtain through Computational Fluid Dynamics (CFD) software, the emission and performance results of E10 and gasoline when used in the same internal combustion engine at the same engine speeds (RPM).

Specific objectives

- Compare the power and torque curves between gasoline and E10 throughout the entire speed range.
- Compare the Indicated Mean Effective Pressure (IMEP) of each fuel throughout the entire speed range.
- Compare the Indicated Specific Fuel Consumption of each fuel throughout the entire speed range.
- Compare the thermal efficiency of each fuel throughout the entire speed range.
- Analyze the behavior of CO, CO_2 Unburnt Hydrocarbons, NO_x, and Volatile Organic Compounds emissions for both fuels throughout the entire speed range.
- Compare the CO, CO_2 Unburnt Hydrocarbons, NO_x, and Volatile Organic Compounds emissions of both fuels throughout the entire speed range.

Scope and limitations of the work

In this work, an internal combustion engine (ICE) using gasoline and E10 as fuels will be simulated to study the performance and emissions characteristics. The engine will be simulated using Ansys Forte, a Computational Fluid Dynamics (CFD) software known for its capabilities regarding ICE simulation. The engine is a spark-ignited engine made by Volkswagen. The specifications of this same engine will be included in Chapter 2.

Likewise, this work will be limited only to the above-described. That is, only simulations with gasoline and E10 will be done; no tests will be done with any other type of alcohol (methanol, butanol, etc.) nor will simulations be done with a blend percentage higher than 10%. This is because only the characteristics and effects on performance and emissions

of ethanol, mainly E10, have been analyzed. Although the reasons why certain pollutants are produced will be explained briefly, we will not go into detail about chemical reactions, chemical kinetics, or the mechanisms of formation of these pollutants.

Hypothesis

The most important statement that must be verified is that E10 should produce fewer emissions in CO_2, CO, and unburnt hydrocarbons than gasoline; but more emissions in NO_x. To do so, CFD simulations with E10 and gasoline will be made and their emissions results will be compared.

General methodology

For the analysis, the geometry will be modeled in CATIA using the scanned piston of a real engine. All the necessary initial data and boundary conditions will be set in the solver. This information includes the composition of E10, an appropriate chemistry model for each fuel; proper mesh refinements, spark ignition settings, and flame settings; dimensional data of the engine such as bore, stroke, and connecting rod length; thermal boundary conditions; initial conditions such as temperature, pressure, and turbulence; and simulation controls that set the beginning and end of the simulation, as well as the engine RPMs. Additional settings include chemistry solver options, time step options, and output controls.

Once the simulations have finished, the emissions and performance results of gasoline and E10 will be analyzed and compared. Additionally, the results of E10 will be compared with those obtained by other authors to validate the use of this numerical technique (CFD).

Chapter 1

Throughout the years, many tests have been made with engines using different fuels. Some to understand the effects on performance, and others to understand their effects on emissions. In this chapter, the effects of ethanol addition on gasoline and previous work done by several authors will be presented. But to understand what follows, it is of utmost importance to explain the principle of operation of a spark-ignition internal combustion engine, performance factors, vital components, emissions, thermodynamics, and related concepts.

Operation principle of the internal combustion engine

The gasoline, or spark-ignition, internal combustion engine operates on the Otto cycle and relies on external ignition for combustion. This ignition, provided by a spark plug, is what burns the air/fuel mixture in the cylinder. Through combustion, the chemical energy in the mixture is now converted into useful mechanical energy (Hofmann, Mencher, Häming, Hess, 2015, p. 8).

Historically, this air/fuel mixture was formed in the carburetor and then moved through the intake manifold toward the cylinder. Nowadays, gasoline direct injection is the norm due to the ever-increasing environmental regulations. The benefits of this novel system are that it allows for an exact measurement of the fuel used at every moment, better fuel economy, and higher power output (Hofmann *et al* 2015, p. 8).

The combustion of the air/fuel mixture causes a reciprocating motion in the piston, this motion is converted into rotary motion by a connecting rod (con-rod) mounted on the crankshaft. This rotational movement is maintained at the end of the crankshaft by a flywheel.

The rotational speed of the crankshaft is the engine speed measured in RPMs (Hofmann *et al* 2015, p. 8).

The Otto cycle consists of four strokes: induction, compression, power, and exhaust. The figure below illustrates each stroke:

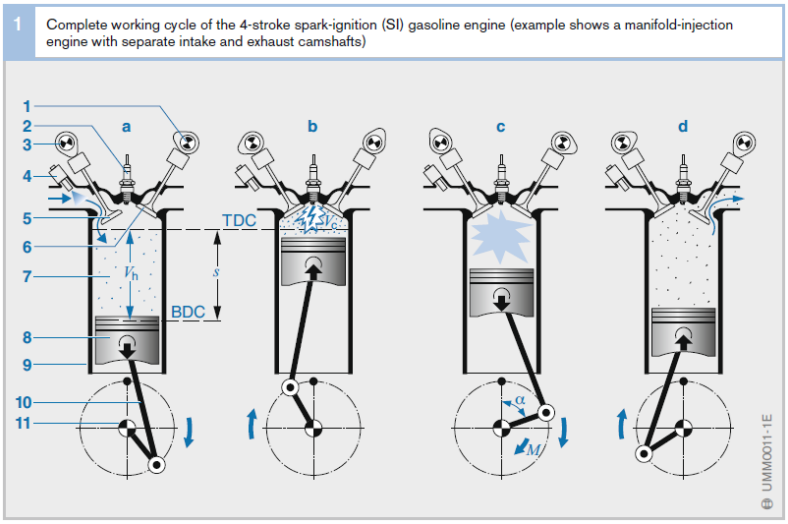

Figure 1. The four strokes of the Otto cycle. Source: Hofmann *et al* (2015)

Where **a** is the induction stroke, **b** is the compression stroke, **c** is the power (or combustion stroke), and **d** is the exhaust stroke. The numbers refer to the different components involved. Number 1 is the exhaust camshaft, 2 is the spark plug, 3 is the intake camshaft, 4 is the injector, 5 is the intake valve, 6 is the exhaust valve, 7 is the combustion chamber, and 8, 9, 10 and 11 are the piston, cylinder, conrod, and crankshaft respectively. TDC is Top Dead Center, BDC is Bottom Dead Center, M is torque, α is the crankshaft angle, s is the piston stroke (simply referred to as stroke), V_h is the piston displacement (useful volume for the work of the piston), and V_c is the compression volume (volume at TDC) (Hofmann *et al* 2015, p. 8).

During the induction stroke, the piston moves downwards causing the volume of the cylinder to increase. During this expansion, fresh air is drawn into the cylinder through the intake valve. The cylinder volume is maximum when the piston reaches BDC. During the compression stroke, both valves are now closed and the piston moves upwards reducing the volume of the cylinder. Before the end of this stroke, fuel is injected to be later ignited. The cylinder volume is at its minimum at TDC (Hofmann *et al* 2015, p. 9).

During the power stroke, the air/fuel mixture is ignited by the spark plug. This combustion causes a rapid increase in pressure and heat in the cylinder, which causes the piston to move downwards. Finally, during the exhaust stroke, the exhaust valve opens before BDC allowing the hot exhaust gases from combustion to exit. While the piston is moving upwards (due to inertia), the remaining gases are pushed out of the cylinder. The cycle begins again with the induction after two revolutions of the crankshaft (Hofmann *et al* 2015, p. 9).

Performance factors of the engine

One of the most important design factors of an internal combustion engine is the compression ratio. It determines the torque and power generation, fuel economy, and emissions of pollutants (Hofmann *et al* 2015, p. 10). It is defined as the ratio between the maximum piston displacement V_h and the compression volume V_c:

$$\varepsilon = \frac{V_h + V_c}{V_c} = 1 + \frac{V_h}{V_c} \tag{1}$$

It is important to note that, as the compression ratio increases, so will the possibility of incomplete combustion. This event is known as detonation and more commonly, as fuel knock. This phenomenon is accompanied by a “pinging” noise, hence its name. It occurs

when “portions of the mixture ignite before being reached by the flame front” (Hofmann *et al* 2015, p. 22). The immense heat and pressure generated during combustion knock subject the engine and its components to intense thermal and mechanical loads, loads that can damage and even destroy the engine (Hofmann *et al* 2015, p. 22).

Some of the causes that can affect the tendency to knock are a significant ignition timing advance, high cylinder-charge density, fuel grade, excessively high compression ratio, ineffective cooling, and combustion chamber geometry. A hefty advance in ignition timing produces high combustion chamber temperatures as well as ineffective cooling. A high cylinder-charge density and an excessively high compression ratio can cause high temperatures during compression, with the added detriment of high pressures too due to the high compression ratio. Fuel grade is also important because the higher the octane rating, the better its resistance to knock. The last concerning cause is the combustion chamber geometry. Poor turbulence and swirl are a product of this (Hofmann *et al* 2015, p. 22).

Returning to the performance factors of the engine, we have the stoichiometric ratio of air to fuel. This relationship known as the air/fuel ratio, indicates the proportion of air to gasoline necessary for the complete combustion of an air/fuel mixture. For gasoline, this ratio is 14.7 to 1, meaning that 14.7 kg of air is needed for the complete combustion of 1 kg of gasoline. The Lambda factor, on the other hand, indicates the relationship between the inducted mass of air and the theoretical air required (Hofmann *et al* 2015, p. 10). It is defined as:

$$\lambda = \frac{induction\ air\ mass}{theoretical\ air\ requirement} \tag{2}$$

A stoichiometric ratio is equal to 1 ($\lambda = 1$). Deviations from this value indicate a rich or lean mixture of air and gasoline. For rich mixtures, where there is more gasoline than air, lambda is less than 1 ($\lambda < 1$); and for lean mixtures, where there is more air than gasoline, lambda is greater than 1 ($\lambda > 1$) (Hofmann *et al* 2015, p. 10).

Besides the Lambda factor and the compression ratio, many other factors have a decisive impact on the performance of the engine. One of them is the cylinder charge, which is the gas mixture trapped in the combustion chamber when the intake valve closes, and it is comprised of fresh and residual gas. Fresh gas is the "fresh air drawn in and the fuel entrained with it", and residual gas is the "portion of the cylinder charge which has already taken part in the combustion process" (Hofmann *et al* 2015, p. 12).

The gas exchange process is measured through the volumetric efficiency, air consumption, and retention rate. This process consists of replacing the consumed cylinder charge with fresh gas. The volumetric efficiency is the ratio of air trapped in the cylinder to the theoretical maximum. For naturally aspirated engines, this ratio lies between 0.6 and 0.9. The air consumption is the total throughput of air mass participating in the gas-exchange process, and the retention rate is the ratio between the volumetric efficiency and the air consumption, or the proportion of the air-mass throughput remaining in the cylinder at the end of the gas exchange process (Hofmann *et al* 2015, p. 13 – 14).

The power that an internal combustion engine can deliver depends on the clutch torque (simply referred to as 'torque') and the engine speed. "The clutch torque is the torque developed by the combustion process less friction torque, pumping losses and the torque needed to drive auxiliary equipment" such as A/C compressors or alternators (Hofmann *et al*

2015, p 16). The combustion torque generated during the power stroke is determined by the air and fuel mass in the cylinder after the closing of the intake valve, and the ignition timing of the spark plug (Hofmann *et al* 2015, p 16).

Torque is the product of a force and a distance (or lever arm). In this case, the force is the one produced during combustion which pushes the piston downwards, and the lever arm is the distance between the center of the crankshaft to the center of the connection point between the crankshaft and the con-rod (crankpin or rod-bearing journal), also known as crankshaft radius. Figure 2 illustrates this:

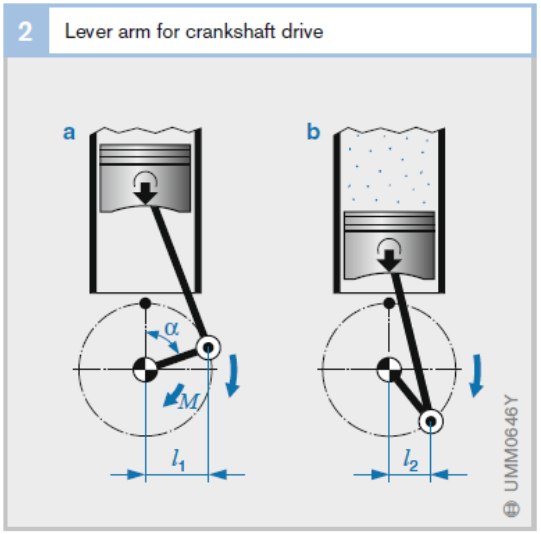

Figure 2. Lever arm for the torque generation. L1 and L2 represent the lever arm. Source: Hofmann et al (2015).

As seen in Figure 2, the lever arm changes with the crankshaft angle (simply referred to as 'crank angle'). This means that torque is not constant throughout the whole combustion cycle. As a consequence, torque is equal to 0 when the piston reaches BDC and TDC.

To determine the power output the following expression can be used (Beer, Johnston, Dewolf, Mazurek, 2009, p. 165):

$$P = T\omega \tag{3}$$

Where P is power in Watts (N*m/s), T is torque in N*m, and ω is the angular velocity in radians per second. It seems that from this equation alone, power will increase indefinitely as torque and engine speed increase too. However, that does not happen in reality. Torque varies according to engine speed and the latter cannot increase infinitely.

As engine speed increases, torque also increases and then hits a maximum value before dropping. At higher engine speeds, the shorter opening of the intake valves limits the cylinder charge, thus diminishing power generation (Hofmann *et al* 2015, p 17). Figure 3 shows typical torque and power curves as a function of engine speed:

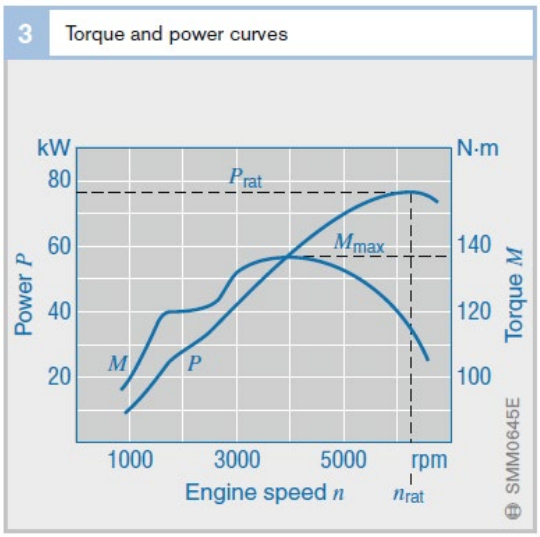

Figure 3. Typical torque and power curves for a manifold-injection engine. Source: Hofmann et al (2015).

In figure 3, n_{rat} is the speed (rated speed) at which peak power (rated power) P_{rat} is obtained. M_{max}, on the other hand, represents the point where maximum torque is reached.

Another important factor is specific fuel consumption. Normally, fuel consumption is measured in liters per 100 km or miles per gallon (mpg). However, it is not very precise.

Therefore, specific fuel consumption provides a more accurate measurement, since it is the ratio of mass of fuel needed (in kg if SI units are used) to produce a certain amount of energy (kW*h). Two parameters have effects on the specific fuel consumption: the lambda factor (λ) and the ignition timing (Hofmann *et al* 2015, p 20).

During rich mixtures, the specific fuel consumption is very high due to the lack of oxygen. It then lowers when lambda equals 1 and then reaches a minimum when the lambda value is between 1 and 1.1; indicating a slightly lean mixture (Hofmann *et al* 2015, p 20). If lambda continues to increase (leaner mixtures), specific fuel consumption will increase too. This is because of the 'lean-burn limit', which is where incomplete combustion occurs (Hofmann *et al* 2015, p 20). Ignition timing, on the other hand, consists of setting the time at which ignition will occur in the cylinder relative to the piston position and crankshaft angular velocity (Zareei, Kakaee, 2013, p. 109).

Exhaust emissions and catalytic conversion

The stoichiometric ratio is a very important factor when defining the amount and type of pollutants emitted. The main constituents of exhaust gas are water, carbon dioxide (CO_2), and nitrogen in its diatomic form (N_2). The typical pollutants after the combustion of gasoline are carbon monoxide (CO), hydrocarbons (HC), nitrogen oxides (NO_x), and sulfur dioxide (SO_2) (Köhler, Allgeier, 2015, p. 261 – 262).

Carbon monoxide is produced when there is an incomplete combustion of rich air/fuel mixtures due to an air deficiency. Hydrocarbons are produced because of an incomplete combustion of the air/fuel mixture due to an oxygen deficiency too. Some of the most common nitrogen oxides produced during combustion are nitrogen oxide (NO), nitrogen

dioxide (NO_2), and nitrous oxide (N_2O). Sulfur dioxide is produced due to the sulfur content found in fuels and although it is not regulated like the others, it must be avoided because it can damage the catalytic converter, reducing its pollutant conversion capabilities (Köhler, Allgeier, 2015, p. 262).

All of these pollutants represent health risks during prolonged exposure. CO inhibits the absorption of oxygen in the blood, some hydrocarbons such as aldehydes are carcinogenic, and nitrogen oxides along with sulfur dioxides produce smog and acid rain (Köhler, Allgeier, 2015, p. 262).

To control and further reduce the aforementioned pollutants, a catalytic converter is used. The most common way of treating exhaust gases is with a three-way catalytic converter. When the engine is operating with rich mixtures, nitrogen oxides (NO_x) are reduced by HC and CO, but these two gases are released to the atmosphere untreated due to the lack of oxygen. On the other hand, if the engine operates on lean mixtures, HC and CO are oxidized by the oxygen available in the exhaust gas and NO_x are released untreated. The maximum conversion rate of pollutants happens during a stoichiometric mixture ($\lambda = 1$) (Frauhammer, Schenck zu Schweinsberg, Winkler, 2015, p. 270).

Another common and possible byproduct of combustion is Volatile Organic Compounds (VOC). These are a type of organic chemical compounds that evaporate with ease (ATSDR, 2008). Many of these compounds are found in gasoline and include but are not restricted to benzene, ethylene glycol, formaldehyde, methylene chloride, tetrachloroethylene, toluene, xylene, and 1,3-butadiene (Minnesota Department of Health, 2022, par. 2).

Fuel supply

Fuel delivery with gasoline direct injection is more complicated than with manifold injection because of the very small timeframe available for doing so. For this reason, the timing of injection, ignition, and mixture preparation has to be very precise. The fuel system is divided into two parts: a low and a high-pressure circuit, and there are two types of systems: continuous-delivery and demand-controlled. Figure 4 shows a schematic of the continuous-delivery system and its parts:

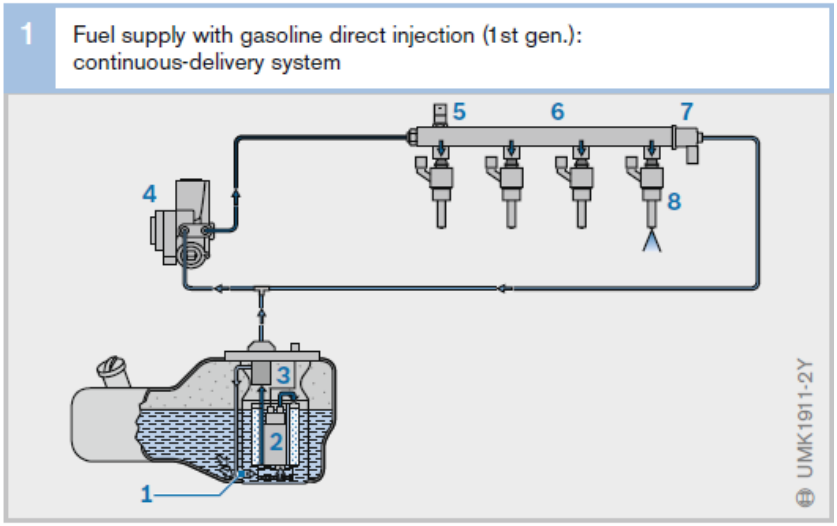

Figure 4. Continuous-delivery system for the fuel supply of gasoline direct injection. Source: Wolber, Schelhas, Müller, Baumann, Keller (2015).

In Figure 4, the numbers indicate the following components: suction-jet pump (1), electric fuel pump with filter (2), pressure regulator (3), HDP1 high-pressure pump (4), high-pressure sensor (5), fuel rail (6), pressure-control valve (7), and the high-pressure fuel injectors (8) (Wolber *et al* 2015, p. 78).

In the continuous-delivery system, fuel is constantly put in the rail at high pressure. The spare fuel that is not needed for injection is depressurized by the pressure-control valve (7) and returned to the low-pressure circuit. The Engine Control Unit (ECU) then actuates the valve to obtain the needed pressure for a given operating point. The problem with these systems is the continuous flow of fuel back and forth from the fuel rail to the pressure-control valve (7) when fuel is not needed anymore. This causes a higher energy consumption from the system and thus, higher fuel consumption (Wolber *et al* 2015, p. 79).

Figure 5 now shows the arrangement for the demand-controlled system:

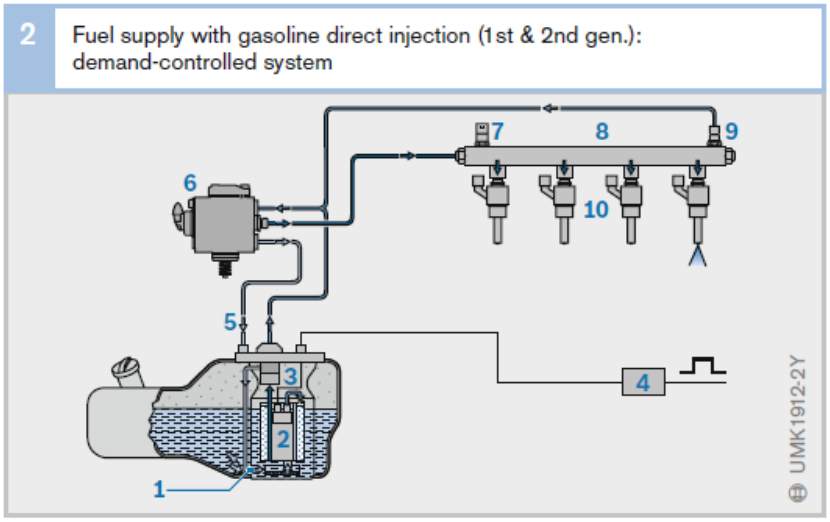

Figure 5. Demand-controlled system for the fuel supply of gasoline direct injection. Source: Wolber *et al* (2015).

Here the components are listed as follows: suction-jet pump (1), electric fuel pump with filter (2), pressure-relief valve and pressure sensor (3), clock module for controlling electric fuel pump (4), leakage line (5), HDP2 high-pressure pump (6), high-pressure sensor (7), fuel rail (8), pressure-limiting valve (9), and the high-pressure fuel injectors (10) (Wolber *et al* 2015, p. 78).

In this system, the amount of fuel supplied to the rail is only the necessary for injection. The supply is regulated through a fuel supply control valve which in turn is actuated by the engine control unit. This secures the necessary system pressure of any given operating point. For safety reasons, this high-pressure circuit features an integrated mechanical pressure-limiting valve mounted on the fuel rail. If the pressure exceeds the allowable level, fuel is then returned to the low-pressure circuit through the aforementioned valve (Wolber *et al* 2015, p. 79).

In both types of systems, the high-pressure pumps are driven by the camshaft. The main difference relies on the type of pump used on each system. For the continuous-delivery system, there is a three-barrel radial piston pump; whereas for the demand-controlled system, there is a single-barrel radial piston pump (Wolber *et al* 2015, p. 79).

Gasoline direct injection

Direct injection to the cylinder was a great technological breakthrough. It allowed greater efficiency and lower fuel consumption when compared with manifold injection, although with greater complexity. The fuel pressure for direct injection is higher and the time window for it is far smaller than with manifold injection.

Binder, Ecker, Glaser, and Müller (2015, p. 110) provide a great explanation of how this high pressure is achieved:

> The electric fuel pump delivers fuel to the high-pressure pump at a pre-supplied pressure of 3...5 bar. The latter pump generates the system pressure depending on the engine operating point (requested torque and engine speed). The highly pressurized fuel flows into and is stored in the fuel rail.

In gasoline direct injection, combustion depends on the injection point, moment of ignition, and the geometries of the combustion chamber and the intake manifold. The two main combustion processes concerning gasoline direct injection are homogeneous and stratified charge. For homogeneous combustion, a stoichiometric mixture is formed ($\lambda = 1$) and expensive exhaust-gas treatment of NO_X is avoided. This process aims to reduce emissions (Binder *et al*, 2015, p. 111).

In the case of stratified-charge combustion, fuel is first injected at a small load and low engine speed into the combustion chamber during the compression stroke, then transported as a stratified-charge cloud to the spark plug. This cloud is ideally surrounded by pure fresh air, which means that the Lambda factor is greater than 1 (Binder *et al*, 2015, p. 112). For stratified-charge combustion, there are two types of processes: wall/air-guided and spray-guided.

In the wall-guided process, the mixture is transported via the piston recess; while in the air-guided process, the mixture "guides the airflow in the combustion chamber in such a way that the fuel is directed on an air cushion to the spark plug" (Binder *et al*, 2015, p. 112). This airflow can exist in a swirl or tumble configuration. In the case of a swirl air flow, the air drawn in from the intake valve generates a turbulent rotational flow along the cylinder wall. On the other hand, a tumble airflow means that the air's movement from top to bottom "is deflected by a pronounced piston recess so that it then moves upwards in the direction of the spark plug" (Binder *et al*, 2015, p. 113).

As for the spray-guided process, the injector is located centrally at the top of the combustion chamber and the spark plug is located below it on the side of the intake valve.

The advantage is that the fuel spray is directly guided towards the spark plug without having to take any deviations. The downside is that there is even less time for mixture preparation; without mentioning the very high pressures needed for injection (200 bar approx.). If this method is properly configured, efficiency and fuel consumption savings are greater than with the wall/air-guided combustion process (Binder *et al*, 2015, p. 113).

With regards to engine operating modes, there are also two main ones: homogeneous mode and stratified charge mode. These are set by the ECU and depend on the engine operating point. The first one is the homogeneous mode. In this mode, Lambda is set to 1 and fuel is injected during the induction stroke to ensure there is sufficient time for a homogeneous mixture (Binder *et al*, 2015, p. 114).

For an air-fuel mixture to be homogeneous, all the gasoline from the previous combustion must have evaporated completely. This evaporation is affected by the temperature of the combustion chamber, the size of the fuel droplet, and the time available for evaporation. During mixture formation in homogeneous mode, “the intake air helps the fuel to evaporate quickly and ensures that the mixture is well homogenized” (Binder *et al*, 2015, p. 117). Figure 6 illustrates the mixture-formation mechanism for this operating mode:

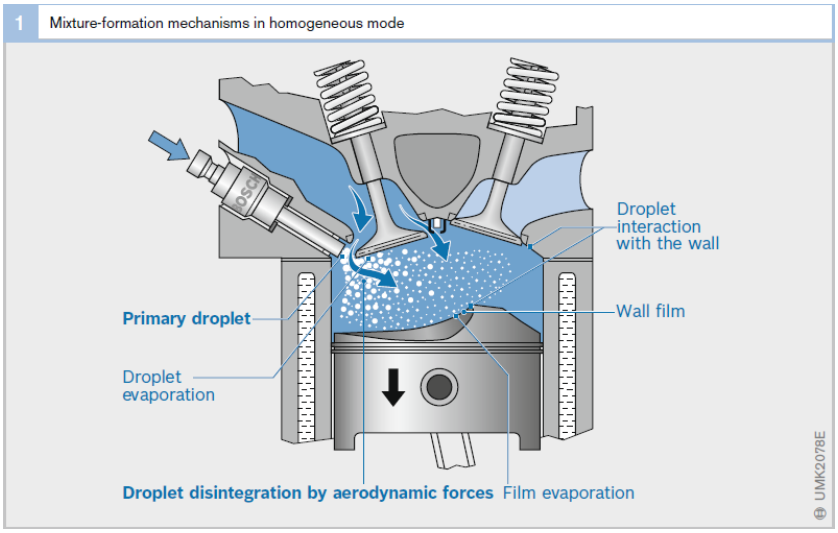

Figure 6. Mixture-formation mechanism for homogeneous mode. Source: Binder *et al* (2015).

Regarding stratified-charge mode, fuel is injected during the compression stroke and a stratified-charge cloud should be surrounded almost entirely by fresh air. Due to this, the mixture tends to be very lean (Binder *et al*, 2015, p. 114). Also, this mode is only used in a very specific range. The engine load cannot be too high because otherwise soot and/or NO_x emissions and fuel consumption would increase drastically. Nor can it be too low because then the exhaust temperatures would be too low and the catalytic converter would not be able to operate solely on these exhaust gas temperatures. In addition, above 3000 RPM time is not sufficient to homogenize the stratified charge cloud (Binder *et al*, 2015, p. 115).

Furthermore, the mixture is only homogeneous in a limited area and the rest of the combustion chamber is filled with inert gas or fresh air. Moreover, fuel is injected during the compression stroke so that the mixture cloud can be transported toward the spark plug by the airflow and the upward movement of the piston. Figure 7 illustrates the mixture-formation mechanism for this operating mode:

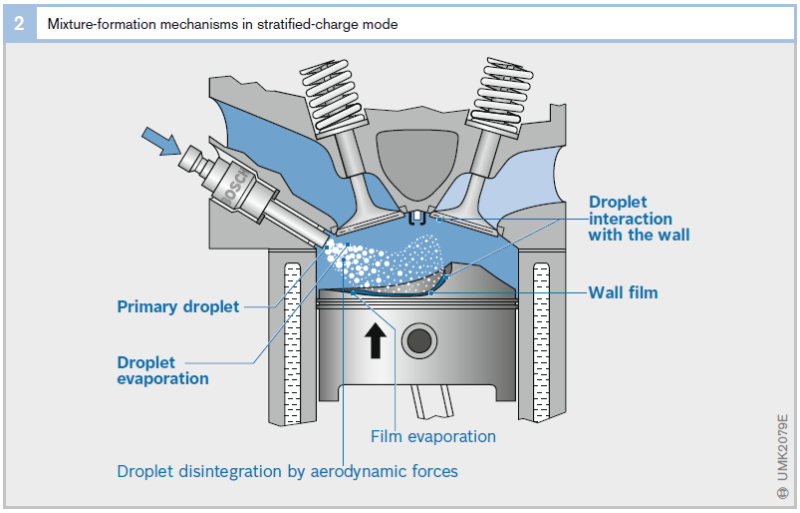

Figure 7. Mixture-formation mechanism for stratified-charge mode. Source: Binder *et al* (2015).

Other engine operating modes consist of variations and combinations of the two main operating modes. To conclude gasoline direct injection, there is the high-pressure injector. Its mission is to measure the amount of fuel going into the cylinder and, through atomization, to achieve a controlled mixing of the fuel and air within it (Binder *et al*, 2015, p. 120).

Thermodynamics of the Internal Combustion Engine

The internal combustion engine, whether gasoline or diesel, does not convert all of the chemical energy contained in the fuel into useful mechanical energy. Part of that energy available during combustion is lost. Some of these losses are thermal, frictional, and due to pumping. Hence, there is a rate of energy conversion or utilization known as thermal efficiency.

To analyze the thermodynamic cycle of an internal combustion engine, a model that is frequently used is the air-standard cycle, which consists of a closed cycle that closely resembles that of an actual engine (open cycle) (Borgnakke, Sonntag, 2013, p. 463). In an

open cycle, mass enters and exits the system, but in a closed one, mass does not exit the system and remains constant.

In an actual engine, the working fluid is comprised of air and fuel that change to combustion products; but in the air-standard cycle, air is the working fluid throughout the whole process (Borgnakke, Sonntag, 2013, p. 462). The air-standard cycle is based on the following assumptions (Borgnakke, Sonntag, 2013, p. 463):

- A constant mass of air is the working fluid during the whole process and air behaves as an ideal gas.
- The combustion process is replaced by a heat transfer process where heat is added by an external source.
- The cycle is completed by heat transfer to the surroundings.
- All processes are reversible.

The only problem with this model is, since it has isentropic processes (processes at constant entropy which are ideal), quantitative results such as thermal efficiency, mean effective pressure, etc. will differ from those of an actual engine. Therefore, this analysis only serves as a qualitative approach to the effect of certain factors on performance.

In the case of the Otto cycle, which corresponds to gasoline engines, the real thermodynamic cycle corresponds to the process previously described in Figure 1. The P-v diagram (Pressure – specific volume) is as follows:

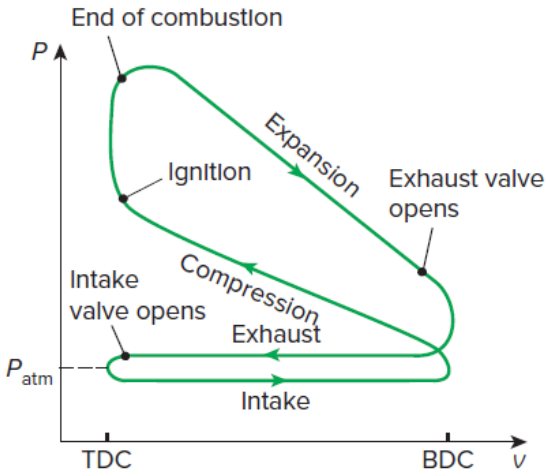

Figure 8. P-v diagram of the real Otto cycle. Source: Çengel, Cimbala, Turner (2017).

For the air-standard Otto cycle, the process is further simplified, and only four states (four different values of mainly pressure and temperature) are identified.

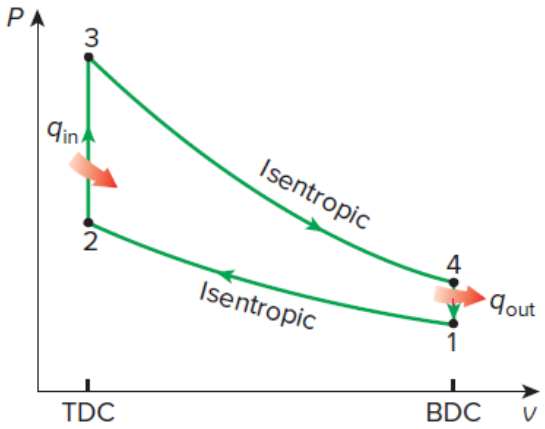

Figure 9. P-v diagram of the air-standard (ideal) Otto cycle. Source: Çengel, Cimbala, Turner (2017)

The process that goes from state 1 to state 2, consists of an isentropic compression (piston travels to TDC) of air. From state 2 to state 3, there is a heat addition (combustion) at constant volume, state 3 to state 4 is an isentropic expansion (power stroke), and during state 4 to state 1 a heat rejection (loss) to the surroundings occurs at constant volume (Çengel, Cimbala, Turner, 2017, p. 352).

Although the air-standard analysis yields only qualitative results, there is some correlation with reality. Using an additional assumption called ‘cold air’, where the air is evaluated at 300 K and the specific heats at constant pressure and constant volume remain constant, the thermal efficiency rises as the compression ratio increases. As compression is higher in the cylinder, so is the pressure generated, this means that the area in the P-v diagram is greater and so will be the useful work produced by the engine. However, it is important to remember that there is an upper limit on the compression ratio that can be used since higher compression ratios lead to a greater probability of knocking in the engine.

As mentioned earlier, the conversion of the chemical energy contained in the fuel into mechanical energy is not complete due to various losses. Primary concerns include thermal, pumping, and frictional losses; while lower concerns refer to losses for a stoichiometric ratio ($\lambda = 1$) since efficiency is highest in lambda values ranging from 1.1 to 1.3 (Hofmann *et al* 2015, p 18 – 19).

Thermal losses happen due to the heat transfer from the fuel to the cylinder walls after combustion. This excess heat is radiated into the environment and lost. These losses also come from the exhaust gas. Pumping losses arise during the 1st and 4th strokes since work is involved when drawing air into the cylinder and when the exhaust gases are pushed outwards through the exhaust port (Hofmann *et al* 2015, p 19). Frictional losses occur due to all the moving parts in the internal combustion engine and auxiliary equipment: the piston ring with the cylinder walls, bearing friction, and that of the alternator drive (Hofmann *et al* 2015, p 19).

Properties of fuels and alternative fuels

The fuel mostly used for spark-ignition engines is gasoline, which is primarily composed of paraffins and aromatic compounds (Ullmann, Allgeier, 2015, p. 24). There are two types of gasoline mainly sold on the market, one is called ‘regular’ and another is called ‘super’ or ‘premium’. There are many differences between them, with the most recognizable one being the octane rating or octane number. The octane rating indicates how susceptible is any given fuel to knock. The higher it is, the lower the possibility of knock in the engine. On the contrary, if the octane rating is very low, it means that engine knock will be very likely.

To obtain the octane rating, a scale going from 0 to 100 is used. Iso-octane, which is very knock-resistant, has a value of 100; while n-heptane (very prone to knock) has a value of 0 assigned to it. The octane rating is obtained by comparing a mixture of iso-octane and n-heptane that displays similar properties to any fuel that will be tested in an engine. The proportion of iso-octane (% by volume) in this mixture which displays similar knock characteristics to the test fuel, indicates the octane rating (Ullmann, Allgeier, 2015, p. 25). Another way to determine the octane rating is by obtaining the average between the Research Octane Number (RON) and the Motor Octane Number (MON).

The RON indicates how much knock can be produced during acceleration, while the MON indicates the knock tendency of the fuel at high engine speeds. Since the Motor method uses preheated mixtures, higher engine speeds, and even variable ignition timing (high thermal demands); the MON will always be lower than the RON (Ullmann, Allgeier, 2015, p. 26). One of the ways to increase the octane rating is by adding oxygenated components.

Other than offering great knock resistance, a high-octane fuel allows for higher compression ratios; which in turn increases thermal efficiency.

Besides the octane rating, the most important property is the calorific value (or heat value) of the fuel. This refers to the available heat in the fuel during full combustion. Related to this, is the calorific value of the air/fuel mixture, which greatly determines the engine's power output (Ullmann, Allgeier, 2015, p. 25).

Beyond conventional fuels such as gasoline and diesel, there are also alternative fuels. These fuels are classified as such because they are not, necessarily, petroleum byproducts (except for liquefied petroleum gas or LPG and natural gas). Some of them are produced using renewable sources of energy, such as biomass. The intention of using these fuels is to eventually replace conventional fossil fuels to reduce pollution. Some examples include natural gas, liquefied petroleum gas (LPG), alcohol fuels, and hydrogen.

The case for biofuels is that they, theoretically, 'recycle' the CO_2 after their combustion. The CO_2 captured by the plants during photosynthesis is now placed back in the atmosphere when these biofuels are burned, therefore, making biofuels a 'carbon neutral' fuel, per se. In reality, this is not the case; since the amount of CO_2 absorbed by the plants and transformed into energy is lower than the CO_2 emitted from combustion in engines (Stan, 2017, p. 151 – 153). According to Stan (2017, p. 153), in Brazil "CO_2 recycling between sugar cane cultivation and the emission from combustion in car engines is estimated at 60%".

Ethanol as a fuel

Due to ethanol's higher oxygen content (and better anti-knock performance), engines must be designed with higher compression ratios to improve thermal efficiency and with it, fuel efficiency as well. It is worth noting that the autonomy that ethanol and its blends with gasoline can provide, is less than with pure gasoline. This is because alcohol is an oxygenated fuel, which is characterized by having oxygen present in its molecular structure.

The lower calorific value of ethanol is because “the oxygen bonded in them does not contribute to the combustion process” (Ullmann, Allgeier, 2015, p. 25). Nonetheless, it does affect the leanness of the air/fuel mixture. Furthermore, the air requirement for ethanol and its blends with gasoline is less. This depends on the molecular structure of the fuel. Due to the lower air requirement, the stoichiometric ratio of air to fuel contributes to a leaner mixture. As Stan states, “the lower the stoichiometric air requirement, the greater the fuel mass”. That is why fuel consumption with ethanol and its blends is higher than with gasoline (2017, p. 158 – 159).

An important property to consider is the enthalpy of vaporization or latent heat of vaporization (as some authors call it). This is defined as “the amount of energy needed to vaporize a unit mass of saturated liquid at a given temperature or pressure” (Çengel *et al*, 2017, p. 115). Other authors define it on a molar basis, but essentially it refers to the energy required by the substance to change from a liquid to a gaseous phase. When compared to gasoline, ethanol’s enthalpy of vaporization is 3.1 times higher. For gasoline direct injection, this represents an advantage due to the higher compression ratios that can be used and the

air-cooling effect produced within the cylinder as a result of this high fuel vaporization (Stan, 2017, p. 159, 174).

Car manufacturers that have tested ethanol as a fuel report having an increase in torque ranging from 10 to 15%. This is because of the increased specific cycle work when combustion occurs faster. This fast combustion tends to be an isochoric process because of the high vaporization enthalpy of ethanol, which is due to the oxygen molecules present in ethanol. Another reason for the torque increase is the lower temperature of air during the intake, which is also due to the vaporization enthalpy of ethanol (Stan, 2017, p. 175).

NO_x emission formation

As covered previously in the 'Exhaust emissions and catalytic conversion' section, it was explained that the main constituents of exhaust gas are water, carbon dioxide (CO_2), and nitrogen in its diatomic form (N_2); and because Earth's atmosphere is composed of 78% nitrogen and 21% oxygen, other pollutants such as carbon monoxide (CO), hydrocarbons (HC), nitrogen oxides (NO_x) and sulfur dioxide (SO_2) are formed after combustion. CO and HC are produced due to incomplete combustion and SO_2 due to the sulfur content in the fuel. NO_x formation, however, is not that simple.

Nitrogen oxides is a term used to group all binary compounds of nitrogen and oxygen. The two most common of these compounds produced during combustion are nitrogen oxide (NO), nitrogen dioxide (NO_2), and nitrous oxide (N_2O) (Köhler, Allgeier, 2015, p. 262), but can also include N_2O_3, N_2O_4, and N_2O_5 (Hoang *et al* 2019, p. 52). NO_x formation is closely related to cylinder pressure, but it is primarily influenced by three factors: the enrichment of oxygen, the reaction time of nitrogen dioxide, and high cylinder temperatures. The emission

of this pollutant "ideally takes place due to the Zeldovich mechanism reaction when the flame temperature is above 1850 K during the combustion" (Rosdi *et al* 2020, p. 2).

Rosdi *et al* are not the only ones who report this, several authors do. Wang, Chen, Ni, Liu, and Zhou (2015, p. 151) agree that NO_x formation takes place at high combustion temperatures, a long residence time at such temperatures, and oxygen enrichment in the reaction regions. Furthermore, Dhande, Sinaga, and Dahe (2021, p. 304) argue that "oxygen concentration and combustion chamber temperature determine NO_x formation". In the same manner, Elshenawy, Razik, and Gad (2023, p. 7, 8) explain that NO_x formation is influenced by the temperature and oxygen content in the combustion chamber and the air/fuel ratio. They add that if cylinder temperatures are above 1800 K, oxygen and nitrogen in the air combine to produce NO_x.

Moreover, Iliev (2021, p. 11) also concurs with what has been said regarding NO_x formation by saying that "high temperature and the presence of free oxygen" are important factors for the formation of these emissions. At the same time, Hoang *et al* (2019, p. 52) assure that NO_x is formed at temperatures over 1500 °C in the combustion process and usually peaks at high temperatures and rich oxygen concentrations (lambda value from 1.1 to 1.2). In addition, Hosseini, Hajialimohammadi, Jafari Gavzan, and Ali Hajimousa (2023, p. 12) establish that NO_x emissions increase with high cylinder temperatures and highlight that at low engine speeds and loads, emissions are the highest.

To summarize, NO_x emissions depend mainly on the temperature achieved in the cylinder during combustion and the oxygen concentration. Additional factors are the reaction time for NO_2, the residence time at high combustion temperatures, and the air/fuel ratio.

Effects of ethanol addition to gasoline on emissions and performance

After explaining some of ethanol's properties and the reasons for NO_x formation, it is important to analyze and understand the effect that ethanol addition has on the performance and emissions of spark-ignition engines, both experimentally and numerically. It is important to mention that the authors report different results regarding performance parameters and emissions, some of which are dependent on the conditions of the experiment, engine specifications, and some others on chemical aspects such as the quality of the fuels used and combustion. Nonetheless, several similarities can help build a complete picture of what to expect when analyzing the results.

From the previous section and the theory explained beforehand, it is known that ethanol increases the octane rating, therefore allowing for the use of higher compression ratios and increasing knock resistance, has a heat of vaporization 3.1 times higher than gasoline, and has a lower calorific value than gasoline. This last point is caused by the oxygen present in ethanol, and even if it does not contribute to combustion, it decreases the stoichiometric ratio and affects the quality of the air/fuel mixture.

Through their experiments, González *et al.* (2018, p. 6) confirmed that the "ethanol enleanment is compensated by means of extra fuel added, normally by means of longer injector time openings". Despite this, they found that the fuel consumption between E10 and the gasoline added with methyl tert-butyl ether (MTBE) showed no statistical differences for the fleet of vehicles used (González *et al.*, 2018, p. 10). In terms of power, they found that for a single-cylinder engine (AVL 5401) the power produced using E10 at constant mass (emulating carbureted vehicles) is lower than using gasoline added with methyl tert-butyl

ether (MTBE), because of the lower heating value and the higher heat of vaporization. At stoichiometric conditions (using fuel injectors), power is almost the same between both fuels (González *et al.*, 2018, p. 8). Emissions of all pollutants were lower in all cases when using E10.

Pham, H., Tuyen, Pham, M., and Le Anh (2015, p. 3) attempted a similar experiment when determining the performance and emissions of carbureted and fuel-injected vehicles using gasoline, E10, E15, and E20. Both cars had an engine displacement of 1.5 L and were first tested at steady-state at full load condition (full throttle) at gear positions 3, 4, and 5 with variations of vehicle speed in each range (Pham *et al* 2015, p. 4). Due to ethanol's higher heat of vaporization, a cooling effect inside the intake manifold was observed and as a consequence, a higher volumetric efficiency was achieved that ultimately led to higher engine power in the carbureted vehicle (Pham *et al* 2015, p. 5).

For the carbureted car, power with the ethanol blends at 4^{th} gear was higher than with pure gasoline. The increment in power at 75 km/h between gasoline and E10 was approx. 12% and 6% on average across all speed ranges. In terms of fuel consumption, the improvement in power led to lower fuel consumption, which was on average 4.6% lower for the ethanol blends (Pham *et al* 2015, p. 5, 6). Furthermore, for the fuel-injected car, at 4th gear and full load both power and fuel consumption had little to no variations Pham *et al* (2015, p. 7). Power with E10 and fuel consumption were slightly higher than with gasoline. The authors explain that the very small changes are due to the equal amount of fuel being injected at all times.

For the emissions of the carbureted car, E10 gave a reduction of 25% for unburnt hydrocarbons (HC's) and 29.6% for CO (Pham *et al* 2015, p. 6). But for NO_x and CO_2 these were 43.7% and 2.2% higher respectively when compared to gasoline. For the fuel-injected car, the emissions of HC and CO were reduced by 3.88% and 7.76% respectively when using E10; but increased by 10.70% and 3.41% for NO_x and CO_2 respectively (Pham *et al* 2015, p. 7, 8). In the end, the authors concluded that the fuel supply system had a considerable influence on power, fuel consumption, and emissions; and that E10 was the best fuel for both vehicles Pham *et al* (2015, p. 9).

Tibaquirá, Huertas, Ospina, Quirama, and Niño (2018, p. 3) also used carbureted and fuel-injected vehicles. In their experiment, they studied analytically and experimentally the effect of low ethanol content (blends up to 20% v/v) on the performance and emissions of sedan-type vehicles without any modification on their ECU. Using a zero-dimensional model, they estimated the power, fuel consumption, and emission of pollutants under different working conditions. Then the same variables were measured on two engines of sedan-type vehicles under laboratory conditions and four different vehicles every 10000 km over the first 100000 km of operation.

In their experiments, Tibaquirá *et al* (2018, p. 4 – 6) measured the specific fuel consumption, power, torque, and emissions index (of CO, CO2, NOx, and Volatile Organic Compounds or VOCs) as a function of RPM, the air-fuel ratio (lambda) and engine load (inlet pressure). Engine 1 has an engine displacement of 1.4 L, compression ratio of 10.2, bore and stroke of 79.8 and 81.8 mm respectively, and indirect fuel injection. Engine 2 had a displacement of 1.6 L, compression ratio of 9.4, sequential multipoint fuel injection. For the

tested vehicles, they used four vehicles. Two of them were carbureted (Chevrolet Sprint, year 1997) and the other two used direct fuel injection (Chevrolet Aveo, year 2010). In their experiments, they used E10 for one carbureted vehicle and one with fuel injection. The Chevrolet Sprint had an engine displacement of 990 cm^3 and a compression ratio of 8.5, while the Aveo had an engine displacement of 1.6 L and a compression ratio of 9.5

The results of their experiment show that CO_2 emissions as a function of lambda increase with higher ethanol content as a result of a more complete and efficient combustion guaranteed by ethanol blends (Tibaquirá *et al* 2018, p. 10). When it comes to CO_2 emission formation, many authors agree that higher ethanol concentration leads to higher emissions because of the more complete combustion produced by ethanol blends. Rosdi *et al* (2020, p. 2) explain that CO_2 is formed by the complete combustion of the fuel, Hoang *et al* (2019, p. 51) declare that the greater oxygen presence from ethanol blends will promote a more complete combustion and the oxidation conversion of CO into CO_2, and Hosseini *et al* (2023, p. 12) establish that CO_2 emissions increase as the ethanol content in the fuel increases.

Back to the results of Tibaquirá *et al* (2018, p. 10), CO emissions were lower in vehicles with carburetor and gasoline direct injection as ethanol content increased. This is a trend observed in research papers by several authors and there seems to be general agreement on one of the reasons why CO emissions decrease when using ethanol blends. The higher the ethanol content in the blend, the lower the CO emissions.

Regarding unburned HC, these had a negligible increment when using E10 compared to gasoline. As for NO_x emissions, the authors state that the production of this pollutant depends on the maximum temperature achieved in the combustion chamber. Since ethanol

has a high enthalpy of vaporization, combustion temperatures in the cylinder are lower than with gasoline, thus reducing the NO_x emissions. As a consequence, these emissions decrease as ethanol content increases (Tibaquirá *et al* 2018, p. 11 – 12). Nevertheless, these results may be very dependent on engine operating parameters and the engine itself because some authors report otherwise.

Wang, *et al* (2015, p. 148, 149) compared the combustion and emissions characteristics of gasoline, a blend of anhydrous ethanol with gasoline (E10) and a blend of hydrous ethanol with gasoline (E10W) under various engine loads. They used a four-cylinder port-injected gasoline engine with a compression ratio of 10.5, a displacement of 1.5 L, and a bore and stroke of 75 and 84.4 mm respectively. The engine was initially run with gasoline to warm up and then ran stably for more than one minute. The engine load ranged from 5 to 100 Nm, and the engine speed was 2000 RPM. The tests were done twice and the result is the average of the two tests.

Contrary to what Tibaquirá *et al* (2018, p. 11) first claimed regarding NO_x emissions, Wang *et al* (2015, p. 151) found that NO_x emissions are higher for blended fuels. Despite the cooling effect offered by ethanol and its blends due to a higher latent heat of evaporation, oxygen makes the mixture leaner, causing the oxidation of nitrogen. Furthermore, the faster combustion and flame propagation by ethanol increases the cylinder temperature, thus increasing NOx emissions.

For HC emissions there was a decrease of 40% and 44.24% for E10W and E10, respectively when compared to gasoline at an engine load of 20 Nm and speed of 2000 RPM (Wang *et al* 2015, p. 152). At higher load conditions, however, these emissions for all three

fuels gradually decrease and almost converge. They explain that HC emission production is primarily caused by unburned mixtures. Also, at low loads, lean mixtures, and low combustion temperatures, HC emissions are caused by flame quenching on the chamber walls.

At 10 Nm of engine load, E10W showed the greatest reduction in CO emissions (Wang *et al* 2015, p. 152). Blended fuels promote a more complete combustion and since CO is produced due to incomplete combustion, these emissions were reduced. CO_2 emissions also were lower for blended fuels in comparison to gasoline. These were lower from 5 to 50 Nm of engine load and at 20 Nm specifically, E10W had an emissions reduction of 39.50% compared to gasoline. The main cause for CO_2 production, as the authors point out, is the carbon-hydrogen ratio of the fuel. By adding ethanol this ratio decreases, hence emitting less CO_2 when using any of the blended fuels.

Unlike previous works, in this paper, an internal combustion engine is simulated. The objective of Iliev's (2021, p. 5) work was to develop a one-dimensional combustion model capable of measuring the performance and emissions of a port fuel-injected (PFI) engine using gasoline and its blends with methanol, ethanol, and butanol. The engine simulation was done on the software AVL Boost, a special program where the user can model a whole engine test bench setup using predefined elements of the software's toolbox. The model had the engine (1), cylinders (4), measuring points (18), plenums (4), system boundaries (2), flow pipes (30), a cleaner (1), flow restrictions (10), and fuel injectors (4) (Iliev, 2021, p. 6).

The combustion model used by the author (Vibe two-zone model) consisted of dividing the combustion chamber into burnt and unburnt zones. The first law of

thermodynamics is applied to the burned and unburned charges respectively. The engine used in the simulations was a four-stroke four-cylinder engine with a compression ratio of 10.5. The bore and stroke were both 86 mm, the connecting rod length 143.5 mm and it had an engine displacement of 2 L. The fuels used were gasoline and blends with methanol, ethanol, and butanol in varying concentrations for the experiment. The blends used were 5, 10, 20, 30, and 50% in volume for methanol, ethanol, and butanol. The engine was simulated at full load condition in the speed range of 1000 to 6500 RPM (Iliev, 2021, p. 7).

One of the disadvantages of using ethanol blends is the lower heating value. Iliev (2021, p. 8, 9) says that engine power decreases with increasing ethanol content and that Brake Specific Fuel Consumption (BSFC) increases as engine speed and ethanol content increase, emphasizing that the reason for the power decrease and BSFC increase when using ethanol blends was the lower heating value; only adding that the lower stoichiometric ratio also played a part in the BSFC increase.

CO emissions decrease significantly as the ethanol content in the fuel increases because the oxygen present in ethanol improves combustion (Iliev 2021, p. 10). Similar results were reached with HC emissions. As ethanol increased, HC emissions decreased and Iliev (2021, p. 10) points out that this happens for the same reasons as for the decrease in CO emissions. In addition, Iliev also found that as the relative air/fuel ratio increased (leaner mixtures), the HC emissions decreased.

For NO_x emissions, Iliev (2021, p. 11) explains that they increase with increasing ethanol content up to 30% throughout the whole speed range, but then decrease when the concentration is 50%. A reason for this, Iliev mentions, is that the improved combustion

increases cylinder temperatures. Iliev also establishes that the decrease in emissions when using 50% ethanol is due to the reduced temperature in the cylinder caused by the much higher latent heat of vaporization of ethanol.

Remembering Wang *et al* (2015, p. 151) experiment, they found that despite the cooling effect offered by ethanol and its blends NO_x emissions were still higher for blended fuels because of the oxidation of nitrogen. Returning to the results of Pham *et al* (2015, p. 8), the NO_x emissions increased by 10.70% with E10 but experienced a reduction of 10.58% with E20. They suggest that a reason might be the lower combustion temperature caused by the greater ethanol concentration. As previously mentioned, with Iliev's (2021, p. 11) findings there is also an increase when using blends up to E30 and a reduction when using E50. This leads to a belief that, perhaps, at low ethanol content the cooling effect is not enough to reduce the cylinder temperatures due to the improved combustion and with it, the NO_x emissions; the reason why at high ethanol concentration there is a reduction in NO_x emissions. Nonetheless, NO_x emissions using any ethanol blend were higher than with gasoline.

Rosdi *et al* (2020, p. 2, 4) studied ethanol-gasoline blends' engine efficiency and emissions characteristics, using gasoline as the reference fuel. The mixtures used were E10, E20, and E30. The experiment was conducted on a spark-ignited turbocharged engine at 40% Wide Open Throttle (WOT) and 3000 RPM. The engine used was a Mitsubishi 4-cylinder, multiport-injection engine. It has an engine displacement of 1.8 L, a bore of 81 mm, a stroke of 89 mm, and a compression ratio of 9.5. To obtain the results, each fuel was tested three times to then report the average values.

Engine performance parameters gave an increase of volumetric efficiency of 6.5% on average for all blends (Rosdi *et al* 2020, p. 4). The individual increase for each blend was 2%, 6%, and 12% for E10, E20, and E30; respectively. They claim that the increased volumetric efficiency is due to ethanol's cooling effect in the intake manifold and the higher octane number. The combustion of ethanol blends is faster and there is a higher peak heat release at high engine speeds.

For Brake Mean Effective Pressure (BMEP), a parameter that reflects engine performance, Rosdi *et al* (2020, p. 5) argue that it is higher with ethanol blends because of the cooling effect produced in the cylinder. This same effect promotes a more complete combustion. Rosdi *et al* (2020, p. 6) state that Brake Specific Fuel Consumption (BSFC) increases proportionally with the ethanol content in the blends because of the lower heating value, higher kinematic viscosity, and the lower air-fuel ratio of ethanol and its blends.

Regarding emissions, Rosdi *et al* (2020, p. 6) report that when using ethanol blends, a trend of NO_x emissions reduction was present with increasing ethanol concentration. Rosdi *et al* agree with what was initially pointed out by Tibaquirá *et al* (2018, p. 11) claiming that when using ethanol blends, the combustion temperature is lower due to the higher heat of vaporization. Rosdi *et al* even declare a reduction of almost 500 ppm of NO_x with E10 compared to gasoline. The results of these two authors suggest that additional reasons for NO_x emissions could be engine operating conditions.

HC emissions in Rosdi *et al* (2020, p. 6 – 7) work were lower as ethanol content increased because of the more complete combustion achieved with ethanol and its blends. HC emissions were 6.6% lower on average. Reasons for HC emissions are “absorption of

fuel vapor into oil layer in cylinder block; flame quenching due to incomplete combustion and filling crevice volumes with the unburned mixture" (Rosdi *et al* 2020, p. 2). For CO_2 emissions, they found a decrease with increasing ethanol content. Rosdi *et al* (2020, p. 2) affirm that CO_2 is formed by the complete combustion of the fuel, and its formation is affected by the carbon-hydrogen ratio of the fuel. For this reason, CO_2 emissions were lower when using ethanol blends.

Meanwhile, Mohammed, Balla, Al-Dulaimi, Kareem, and Al-Zuhairy (2021, p. 3 – 5) performed experiments using gasoline and mixtures of ethanol ranging from 10 to 40% in increments of 10% by volume on a single-cylinder, four-stroke, spark-ignition engine. The engine in question (TD-200) had a compression ratio of 8.5 a displacement of 172 cm^3 and a bore and stroke of 67 and 49 mm respectively. For the experiments they used variable engine speeds from 1500 to 2500 RPM with increments of 250 RPM. Subsequently, each test was performed three times and the value reported is the average of the three.

For the performance results, brake power at all speeds was higher with ethanol blends, the highest of them all being E40 (Mohammed *et al* 2021, p. 5). The leaning effect provided by the ethanol addition increases the air-fuel ratio and brings combustion closer to stoichiometric conditions. This same leaning effect was also reported by González *et al* (2018, p. 6). Furthermore, thermal efficiency also improved with the ethanol blends. The highest value was obtained at 2500 RPM using E40. According to them, this happens because combustion is improved due to the higher flame speed and octane number of ethanol blends.

As opposed to engine power and thermal efficiency, the volumetric efficiency decreased with increasing engine speed and ethanol content. Mohammed *et al* (2021, p. 5)

assure that this is due to less air entering the cylinder at higher engine speeds. At higher engine speeds, the smaller opening time of the intake valves means there is less air in the cylinder. However, 2500 RPM is not that very high of an engine speed. Besides, all of the literature previously revised suggests that ethanol's higher heat of vaporization improves volumetric efficiency. BSFC was also lower with increasing engine speed and ethanol content (Mohammed *et al* 2021, p. 8). The lowest value was at 2500 RPM for E40, for which a decrease of 17.21% in BSFC was reported between E40 and gasoline at 2500 RPM.

Concerning emissions, Mohammed *et al* (2021, p. 8) achieved similar results to those of Rosdi *et al* (2020, p. 6) and Tibaquirá *et al* (2018, p. 11) regarding NO_x. These showed an increasing trend with engine speed, contrary to what Wang *et al* (2015, p. 151) found by claiming that NO_x emissions increase with engine load (which is inversely proportional to engine speed). Based on Mohammed *et al* (2021, p. 8), as load increases, fuel consumption does too and this causes higher temperatures in the cylinder, thus producing NO_x. Even though NO_x emissions increased with engine speed, these decreased with ethanol content. The maximum reduction was recorded with E40 at 1500 RPM.

CO emissions, a product of incomplete combustion, were lower using ethanol blends at all engine speeds (Mohammed *et al* 2021, p. 8). CO_2 emissions, on the other hand, increased at higher engine speeds but decreased with increasing ethanol content, a product of a more complete combustion. The lowest values of CO_2 emissions were those obtained using E40. The authors believe that a possible reason for this is the carbon-hydrogen ratio of the fuel, a fact confirmed by Wang *et al* (2015, p. 152) and Rosdi *et al* (2020, p. 2). For HC emissions, Mohammed *et al* (2021, p. 8) elaborate that increasing the ethanol content in the

blended fuels leads to lower levels of HC emissions because the mixture can be more homogeneous, and more complete combustion can be achieved. At all engine speeds with all blends, HC emissions were lower than with gasoline.

Similarly, Yusaf, Buttsworth, and Najafi (2009, p. 1) performed experiments on a four-stroke spark-ignition engine. To verify the results obtained in their experiments, they made a mathematical model using MATLAB. This model used the first law of thermodynamics and conservation equations to predict the real engine's performance for different ratios of ethanol blends. In their experiments, Yusaf *et al* (2009, p. 2) used a four-cylinder spark-ignition engine from KIA with gasoline and ethanol blends. The ethanol blends ranged from 5 to 20% in volume with increments of 5%. All experiments were done at full throttle. The engine had a displacement of 1.3 L, compression ratio of 9.7, and bore and stroke of 71 and 83.6 mm, respectively.

As ethanol content increases, engine brake power and the indicated mean effective pressure increase too (Yusaf *et al* 2009, p. 3). The very slight power increase is due to ethanol's higher heat of vaporization. This cooling effect leads to a denser cylinder charge. As a consequence of greater ethanol content, torque is greater too; but just slightly. Furthermore, the added ethanol will produce a leaner air-fuel mixture, making combustion more efficient. Also, knock resistance is improved. In the same way, greater ethanol content is also linked to higher thermal and volumetric efficiency. In parallel, the brake specific fuel consumption (BSFC) decreased because of the higher thermal efficiency.

For CO emissions, these decreased as ethanol content increased. This is a consequence of a more complete combustion, the lower carbon content, and oxygen's

presence in ethanol (Yusaf *et al* 2009, p. 3 – 4). The CO concentrations at 3000 RPM decreased by 13.7%, 24.31%, 27.93%, and 45.42%; for E5, E10, E15, and E20 respectively. Based on Yusaf *et al* (2009, p. 4), CO_2 emissions increased proportionally to ethanol content and depended on the relative air/fuel ratio and the concentration of CO emissions. Their results show that at 3000 RPM there was an increase in emissions of 3.87%, 6.06%, 6.76%, and 10.14%; for E5, E10, E15, and E20 respectively. HC emissions, on the other hand, decreased with increasing ethanol content. In the view of Yusaf *et al* (2009, p. 4), the higher the relative air/fuel ratio, the lesser the emissions of this pollutant. At 3000 RPM, emissions decreased 16.94%, 24.04%, 25.14% and 31.69%; for E5, E10, E15, and E20 respectively.

Regarding NO_x emissions, these increased proportionally to the ethanol content (Yusuf *et al* 2009, p. 4). At 3000 RPM, emissions increased by 12.57%, 33.94%, 33.6% and 45.55%; for E5, E10, E15, and E20 respectively. The lean mixtures formed in the cylinder due to ethanol addition make combustion more complete. Because of this, CO_2 emissions will increase and the emissions of CO and unburnt HC will decrease (Yusuf *et al* 2009, p. 6). However, when combustion is closer to stoichiometric conditions, flame temperature increases, and as a consequence, NO_x formation will increase. Dhande *et al* (2021, p. 304) and Iliev (2015, p. 95) agree exactly with this last statement about NO_x formation.

Six years before his research using methanol, ethanol, and butanol, Iliev (2015, p. 87 – 89) only tested with ethanol blends. He developed a one-dimensional combustion model capable of measuring the performance and emissions of a four-stroke port fuel injection (PFI) engine using gasoline, E5, E10, E20, E30, and E50. The engine simulation was done on the software AVL Boost. The model, just as in his future work, had the engine (1), cylinders (4),

measuring points (18), plenums (4), system boundaries (2), flow pipes (34), a cleaner (1), flow restrictions (10), one catalyst and fuel injectors (4). The combustion model and engine used in the simulations were the same as in Iliev (2021, p. 7).

For the simulations, Iliev (2015, p. 92) used gasoline and ethanol blends of varying concentrations for the experiment. The blends used were E5, E10, E20, E30, and E50. The engine was simulated at full load condition in the speed range of 1000 to 6500 RPM with speed increments of 500 RPM.

For engine performance parameters Iliev (2015, p. 93) determined that engine brake power was found to be lower for all ethanol blends at all speeds, a consequence of ethanol's lower heating value. Likewise, engine torque was lower for all ethanol blends at all engine speeds. Despite this, the cylinder charge was cooler and denser because of ethanol's higher heat of vaporization, meaning a higher volumetric efficiency was achieved. Furthermore, BSFC increased as ethanol content increased (Iliev, 2015, p. 94). The reasons for this are the lower heating value and the lower stoichiometric ratio for ethanol and its blends with gasoline.

Concerning emissions, Iliev (2015, p. 94) determined that CO concentration decreased as ethanol percentage increased. The increase of the oxygen proportion promotes further oxidation of CO during combustion. Also, ethanol has less carbon than gasoline. Figure 6.5 presented in the work shows that the lowest emissions were recorded with the E50 blend. On the other hand, NO_x emissions increased with increasing ethanol content in the fuel (Iliev, 2015, p. 95). Iliev highlights that when combustion is closer to being stoichiometric the flame temperature increases, and with it, NO_x emissions.

Referring to HC emissions, these also decrease when ethanol content increases (Iliev, 2015, p. 95). E5 and E10 gave slight reductions compared to gasoline, and E30 was the blend with the lowest emissions results on average across all engine speeds. The most important reasons for HC emissions production are fractions of the charge entering the crevice volumes and not being burned, fuel absorption into the oil layer, and fuel deposition in the cylinder wall during intake and compression (Iliev, 2015, p. 91). Additional causes include quench layers on the combustion chamber wall, occasional partial burning or complete misfire during poor combustion, and "direct flow of fuel vapor into the exhaust system during valve overlap in PFI engines" (Iliev, 2015, p. 91).

Dhande *et al* (2021, p. 298 – 299) used in their research a single-cylinder, spark-ignition, four-stroke engine by Kirloskar that had a bore and stroke of 87.5 and 110 mm respectively; an engine displacement of 661 cm^3 and a compression ratio of 10:1. For the experiment, they performed initial tests at engine speeds from 1300 to 1800 RPM with fixed fuel injector pressure and injection angle to generate the baseline data. Then, further tests were made using ethanol blends, for this, the ethanol used was extracted from pomegranate juice. The ethanol blends used in the tests are E10, E15, E20, and E25. For the evaluation of results, an average of three tests per fuel was done. Additional procedures for the engine testing include starting the engine at a condition of no load for five minutes until it reached a steady state and that the engine was run "for ten minutes to achieve the equilibrium for each test condition before taking the final results" (Dhande *et al* 2021, p. 301). All tests were done under full load conditions.

In terms of engine performance, Dhande *et al* (2021, p. 302) found that when using ethanol blends thermal efficiency drops as engine speed increases. The highest thermal efficiency recorded was 28.33% with the E15 blend at 1500 RPM. The authors believe that a reason for a drop in thermal efficiency as engine speed increases might be the higher octane rating of ethanol and its blends than gasoline. Also, incomplete combustion may lead to lower thermal efficiencies.

Furthermore, at 1600 RPM E10 had 12.12% higher BSFC than gasoline, while E15 was 12.12% lower at 1500 RPM (Dhande *et al* 2021, p. 303). Of all the blends, they determined that E15 had the lowest BSFC at higher speeds. On average, BSFC increases as ethanol content and engine speed increase. In addition, power increased as ethanol content also increased at all engine speeds. According to the authors, the latent heat of evaporation of the blended fuels yields a denser cylinder charge at lower temperatures, increasing the volumetric efficiency and engine power. Nonetheless, engine power while using E10 was lower than with gasoline.

The emissions results of the ethanol blends were promising. HC emissions decreased with increasing ethanol content, since the oxygen content in ethanol improves the mixing of the fuel with the air, resulting in better combustion (Dhande *et al* 2021, p. 303). CO emissions decreased as ethanol content increased, with the only exception being E10. At 1500 RPM the reduction in emissions for E15, E20, and E25 was 88.36%, 90.32%, and 90.89% respectively (Dhande *et al* 2021, p. 304). In the case of CO_2 emissions, these increased with higher ethanol content. Dhande *et al* (2021, p. 304) claim that there is a dependency on combustion and CO emissions. The only ethanol blend with lower CO2 emissions than gasoline at all engine

speeds was E10. At 1700 RPM, CO2 emissions increased using E15, E20, and E25 by 4.17%, 4%, and 5.15% respectively compared to gasoline.

For NO_x emissions, Dhande *et al* (2021, p. 304) state that these increase as ethanol content increases, but decrease with engine speed. At 1700 RPM, E10 gave the lowest results of emissions, with a reduction of 30% against gasoline. At 1800 RPM, however, the other blends all registered increments. E15, E20, and E25 had an increase of 8.88%, 15.72%, and 76.93% in emissions compared to gasoline. This happens because combustion is very close to being stoichiometric, as a result, flame temperature and NOx emissions increase.

In a similar manner to Dhande *et al* (2021, p. 299), Yusuf and Inambao (2021, p. 886) used ethanol produced from *Mbwazirume* peels (a species of African banana) to blend it with gasoline at different ratios. They analyzed and compared the performance and emissions of a single-cylinder engine using E5, E10, E15, and unleaded gasoline. Before collecting the data, the engine ran for some time until it reached steady-state conditions. After reaching steady-state conditions, the engine was ready to perform the experiments. The engine speeds ranged from 1800 to 3000 RPM, at wide open throttle (WOT) and 6.9 ± 0.9 bar for Brake Mean Effective Pressure (BMEP) at ambient temperature. The engine in question was a TD-201 single-cylinder four-stroke engine with electronic fuel injection connected to a dynamometer and exhaust gas analyzers. The engine had a compression ratio of 8.5, a bore of 67 mm, a stroke of 49 mm, and a crankshaft radius of 24.5 mm.

In terms of performance, Yusuf and Inambao (2021, p. 887 – 888) report that Specific Fuel Consumption (SFC) decreased by 11.3% and 15.7% for E5 and E15 respectively between 2400 and 2700 RPM. From what can be seen in Figure 2 presented in their work,

SFC is lower at all speeds for the three ethanol blends except E10. For E10 SFC was almost the same as with gasoline at 2100 RPM and even higher than gasoline at 2400 RPM. With E5 and E15, however, the SFC values reached their lowest point at 2400 RPM compared to gasoline. Brake Thermal Efficiency (BTE), on the other hand, was overall higher for all ethanol blends when compared to gasoline, reaching its highest value at 2700 RPM with E15, which was found to be 6.7% higher than with gasoline.

Engine power was higher at all engine speeds with ethanol blends. The recorded engine power was on average 1.3%, 1.9%, and 2.4% higher than gasoline with E5, E10, and E15 respectively. Factors of this are increased engine speeds, lower calorific value for ethanol blends, and a higher octane number. Yusuf and Inambao (2021, p. 888) suggest that the higher octane number improved combustion at all engine speeds under steady-state conditions. Regarding the torque results, these were higher at all engine speeds for all ethanol blends when compared to gasoline. The highest values of torque and Brake Mean Effective Pressure (BMEP) were recorded between 2400 and 2700 RPM.

For the emissions results, Yusuf and Inambao (2021, p. 890) determined that NO_x emissions were the lowest with E10 at 2700 RPM. The CO_2 emissions diminished as a consequence of the higher ethanol ratio (Yusuf and Inambao, 2021, p. 891). The authors argue that this happens because the oxygen in the blended fuels and the high flammability improves the mixing process. HC emissions decreased when using ethanol blends. All blends showed lower emissions than gasoline; with E10 showing the highest results of HC emissions among them. With CO emissions, E5 produced the highest of them all and E15 the lowest. These emissions occur when there is incomplete oxidation of the fuel in the cylinder. Yusuf

and Inambao (2021, p. 891) conclude that the changes in CO and CO_2 emissions between E5 and E15 are due to the lower stoichiometric ratio of the blended fuels, a result of the oxygen present in their molecular structure.

Instead of using an automobile engine or a research engine, Hoang *et al* (2019, p. 49) used a single-cylinder, four-stroke motorcycle engine that had a displacement of 109.1 cm^3, a compression ratio of 9:1 and a bore and stroke of 50 and 55.6 mm respectively. They studied the emissions and performance characteristics, based on the ECE R40 test cycle, of gasoline, E5, and E10. Emissions and performance characteristics were determined by running the engine from 20 to 80 km/h with increments of 10 km/h at 3^{rd} and 4^{th} gear.

Hoang *et al* (2019, p. 50 – 51) registered the highest values of engine power with E10 throughout the entire speed range in both gear positions. On average, the increase in power at 3^{rd} gear of E10 was 6.52% and 4.01% compared to gasoline and E5 respectively. At 4^{th} gear, the power increase observed by the E10 mixture was 7.41% and 5.85% respectively, compared to gasoline and E5. A reason for this increment in power is the higher volumetric efficiency, which is caused by the greater latent heat of evaporation of E5 and E10, hence, the temperatures in the intake manifold are lower. Regarding fuel consumption, it was lower overall during the whole speed range. For E10 at 3^{rd} gear, it was 4.26% and 1.92% lower compared to gasoline and E5 respectively. At 4^{th} gear, the reported reduction for E10 was 4.24% and 2.10 % compared to gasoline and E5 respectively.

The emissions results show that CO_2 increased with ethanol blends (Hoang *et al* 2019, p. 51 – 52). The greater oxygen presence from ethanol blends will promote a more complete combustion and the oxidation conversion of CO into CO_2. When operating at 3rd gear,

emissions increased with E10 by 13.46% and 6.04% when compared to gasoline and E5 respectively. When operating at 4th gear, these increased 12.32% and 5.98% respectively. CO emissions, on the other hand, experienced an average reduction of 5.24% and 1.85% when using E10 at 3rd gear compared to gasoline and E5, respectively.

Based on the explanation of Hoang *et al* (2019, p. 52), HC emissions depend strongly on engine design, operating conditions, and incomplete combustion. If there is enough oxygen during combustion, there will be a reduction of these emissions. At 3rd gear, HC emissions over the entire speed range were 5.54% and 13.78% lower when using E10 in comparison with E5 and gasoline respectively. At 4th gear, the reduction of HC emissions with E10 was 5.36% and 10.84% compared to E5 and gasoline respectively.

At speeds lower than 60 km/h NO_x emissions tended to decrease, but at higher speeds, the opposite happened (Hoang *et al* 2019, p. 53). The authors suggest that poor combustion with lean mixtures of E5 and E10 at low engine speeds, and the lower calorific value of the ethanol blends are possible reasons for this behavior. At 3rd gear, NO_x emissions using E10 increased by 2.09% and 1.66% compared to gasoline and E5 respectively. At 4th gear, the increase was 2.13% and 1.68% compared to gasoline and E5 respectively. Hoang *et al* (2019, p. 52 – 53) emphasize that in lean conditions, "low combustion temperatures are the primary cause of NO_x emission reduction".

Similar to Iliev, Elshenawy *et al* (2023, p. 3) also simulated an internal combustion engine and studied its performance and emissions using ethanol blends. They developed a quasi-dimensional two-zone thermodynamic mathematical model capable of predicting the performance, combustion, and emission characteristics of a spark-ignition engine using

gasoline and ethanol blends at different engine speeds. The equations used to construct the model in MATLAB were the first law of thermodynamics, energy, and mass conservation, equations of state and mass fraction burned. For the engine combustion modeling, the working fluid was divided into burned and unburned zones, in which there was no heat or work transfer between them. Both zones are perfect gases with different properties and have the same pressure because “the flame is a deflagration combustion wave” (Elshenawy *et al* 2023, p. 3).

The single-cylinder engine used in the simulations had a bore and stroke of 65.1 and 44.4 mm respectively; a connecting rod length of 79.55 mm, and a compression ratio of 7:1, and the fuels used were gasoline, E5, E10, E15, and E20 at engine speeds ranging from 2000 to 2800 RPM (Elshenawy *et al* 2023, p. 5).

Elshenawy *et al* (2023, p. 5) proved that power output increased as ethanol content and engine speed increased. Power output for E5, E10, E15, and E20 were 1.18, 2.6, 4, and 5.5% greater than gasoline, respectively at 2500 RPM. In the same way, engine torque increased. At 2500 RPM the authors registered 4.57, 4.62, 4.69, 4.76, and 4.84 N*m for gasoline, E5, E10, E15, and E20, respectively.

The Mean Effective Pressure (MEP) of the ethanol blends increases slightly with higher ethanol content (Elshenawy *et al* 2023, p. 6). This is because ethanol burns more efficiently, causing a faster flame speed which means more power and a higher MEP. At 2500 RPM, the increase of MEP with the ethanol blends when compared to gasoline was 2.5, 4.1, 6.8, and 8.9% for E5, E10, E15, and E20 respectively.

Furthermore, the lower calorific value of ethanol means that the specific fuel consumption (SFC) will increase (Elshenawy *et al* 2023, p. 6). At 2500 RPM SFC increased 1.9, 3.7, 5.5, and 7.2% for E5, E10, E15, and E20 respectively. With volumetric efficiency, the authors argue that it improves with higher engine speed and ethanol content in the fuel. The higher heat of vaporization of ethanol lowers the temperature of the intake manifold, thus increasing the volumetric efficiency. In terms of thermal efficiency, Elshenawy *et al* (2023, p. 7) found very few reductions when using ethanol blends. From Figure 4 presented in their work, it can be seen that the highest thermal efficiency was achieved at an engine speed very near 2300 RPM. From that point onwards, it decreases with all fuels.

NO_x emissions were lower for all ethanol blends at all engine speeds compared to gasoline and these decreased with increasing ethanol content but increased at higher engine speeds (Elshenawy *et al* 2023, p. 7). The authors seem to contradict themselves because then they explain that if cylinder temperatures are above 1800 K, oxygen and nitrogen in the air combine to produce NO_x (Elshenawy *et al* 2023, p. 8); when prior to their results they state that when using E20 the highest temperature recorded was 2265 K, compared to the 2047 K registered when using gasoline (Elshenawy *et al* 2023, p. 7). This last statement would mean that NO_x emissions should have increased in their experiments.

Moreover, with increasing engine speed, cylinder temperature, and fuel consumption rose, and as a consequence, CO concentration did too. However, these emissions decreased as the ethanol content in the fuel increased (Elshenawy *et al* 2023, p. 8). The biggest reduction in CO emissions compared to gasoline was 23.5% at 2500 RPM when using E20. In addition, HC emissions decrease as engine speed and ethanol content increase. The authors explain

that the better mixing of air and fuel, the higher fuel consumption, and the combustion improvement decrease the HC concentration. At 2500 RPM, the biggest reduction in HC emissions compared to gasoline was 16% when using E20 (Elshenawy *et al* 2023, p. 9).

Contrary to HC and CO emissions, CO_2 increased. Improved combustion and high flammability led to this. Besides, the reduction of CO emissions leads to an increase in CO_2 emissions. The highest increase in emissions of CO_2 with respect to gasoline was 23.5% at 2500 RPM when using E20 (Elshenawy *et al* 2023, p. 10).

Finally, we have the experiment from Hosseini *et al* (2023, p. 3, 4). They used a four-stroke, four-cylinder engine with a compression ratio of 11:1, an engine displacement of 1649 cm^3, and a bore and stroke of 78.6 and 85 mm respectively. The four different fuels used in this study were gasoline, E5, E10, and E15. Before measuring data, the engine was started and run at 2000 RPM for 10 to 20 minutes at 50% throttle until the engine and its parts reached a steady state. Then, the load was progressively increased until it reached a maximum value. The engine speeds at which the fuels were tested were 2000, 2500, and 3000 RPM at full load conditions.

The engine was simulated using GT-Power (Hosseini *et al* 2023, p. 7). For this, models of the intake and exhaust were made. The intake system of the engine consists of four pipes (equal to the number of cylinders) which are connected to a reservoir known as a runner. After going into the reservoir and then the cylinder, the air goes to the runners. The exhaust system consisted of exhaust valves (8), manifolds (4), catalysts, and gas collectors.

Their first performance parameter presented is torque. E10 displays the highest registered torque output at 2000 RPM, but then decreases and is lower than gasoline at 2500 and 3000 RPM. There is not a good correlation between the experimental and numerical results of torque. Engine power results between the experiment and the simulation were almost the same, with little to no differences. E10 and E15 were very closely matched with gasoline in terms of engine power at all speeds (Hosseini *et al* 2023, p. 7). At 3000 RPM and full load conditions, engine power using ethanol blends was found to be 5.79, 1.89, and 1.57% lower than gasoline using E5, E10, and E15 respectively (Hosseini *et al* 2023, p. 10).

Contrary to almost all other authors cited in this thesis work, Hosseini *et al* (2023, p. 8) just like Mohammed *et al* (2021, p. 5), claim that volumetric efficiency is lower with ethanol blends. Also, due to the torque reduction, volumetric efficiency had to be lower. Hosseini *et al* (2023, p. 10) found that gasoline had a volumetric efficiency 6.32, 1.85, and 3.05% higher than E5, E10, and E15 respectively.

In terms of BSFC, E10 was the one that showed the lowest results at all engine speeds and load conditions. At 3000 RPM and full load, BSFC for gasoline was 3.34% lower than E5, but 3.79 and 1.45% higher than E10 and E15 respectively. A reason for the decrease in BFSC with higher ethanol content is, according to Hosseini *et al* (2023, p. 10), that by adding ethanol to the fuel the oxygen content is increased, and better mixing of the fuel with the air is achieved, thus resulting in lower BSFC figures.

Hosseini *et al* (2023, p. 10) assure that CO emissions depend on the amount of unburned fuel in the engine, the engine operating temperature, and the compression ratio. By increasing the ethanol content in the fuel, CO emissions are reduced. At 3000 RPM and full

load, CO emissions were 3.19, 15.21, and 23.46% lower for E5, E10, and E15 respectively when compared to gasoline. On the contrary, CO_2 emissions increase as the ethanol content in the fuel increases (Hosseini *et al* 2023, p. 12). The high latent heat of vaporization of ethanol, the air/fuel ratio, engine speed, and load conditions play a part in CO_2 production. At 3000 RPM and full load, CO_2 emissions were 5.73, 9.71, and 16.03% higher for E5, E10, and E15 respectively when compared to gasoline.

Hosseini *et al* (2023, p. 12) suggest that one cause of HC emissions is engine oil burning. Another reason is that the air/fuel mixture fills the gaps created by the grooves in the piston. Also, when unburned fuel is emitted during combustion, HC is emitted as well. With higher ethanol content, HC emissions decrease because of ethanol's improved ignition chain reaction. Additionally, higher HC emissions mean lower thermal efficiency. At 3000 RPM and full load condition, HC emissions were 19.31, 33.40, and 44.04% lower for E5, E10, and E15 respectively when compared to gasoline.

Regarding NO_x emissions, Hosseini *et al* (2023, p. 12) explain that by adding ethanol to the fuel, NOx emissions increase. At 3000 RPM and full load, these were 12.53, 22.42, and 29.93% higher for E5, E10, and E15 respectively when compared to gasoline.

With all the experiments and simulations of other authors revised and analyzed, it is possible to conclude that, at least for performance, volumetric efficiency with ethanol blends increases. For engine power, torque, BSFC, and IMEP, the majority of authors indicate that these increase when using E10. With thermal efficiency, however, it is not possible to establish an adequate conclusion since there is almost an equal amount of authors that claim that it either increases or decreases using ethanol blends.

In terms of emissions, the vast majority of authors agree that HC and CO decrease with increasing ethanol content and that these are a product of incomplete combustion. Opposed to this, six authors agree that CO_2 emissions increase due to a more complete combustion offered by the ethanol blends; but five agree that these decrease when using ethanol blends.

NO_x emissions, however, are very particular because it was found that they do decrease with increasing ethanol content only if it is high enough (E50, for example). Seven different authors agree that these emissions increase when using E10, but six authors disagree. Furthermore, if the ethanol concentration is too low, the cooling effect offered by the higher heat of vaporization will not be enough to counter the rich oxygen concentration in the cylinder when using ethanol blends. With all of this expressed, it is now possible to know what to expect when performing our simulation.

Chapter 2

Historically, the emissions and performance of engines were determined with physical testing by using a real engine on a test bench or dynamometer. As the technology evolved, newer and more sophisticated methods were born and with the development of computers and numerical methods; engine simulation began. Engine simulation has gained a lot of importance in recent years due to its advantage in reducing costs and time in the prototype phase of design. In this chapter, we will see all that is related to the engine simulation that will be done in this work. It will include a detailed description of the data input in the software, an explanation of parameters, the theory behind the models and tools used in the software, and all the steps covering the geometry to how the simulation was run.

In this work, Ansys Forte was chosen as the simulation environment for the engine. The software was chosen because of its solution methods for discretization, fuel combustion kinetics, mesh control features, and various models for turbulence, heat transfer, spray, spark ignition, and turbulent flame propagation.

Ansys Forte uses spatial and temporal differencing methods to discretize the governing equations, the two of which are based on the Arbitrary Lagrangian-Euler (ALE) method. Then, to solve the algebraic finite volume equations that result from these differencing methods, Ansys Forte uses an implicit method known as the SIMPLE algorithm (Ansys Forte Theory Manual, 2022, p. 29 – 31), which stands for Semi-Implicit Method for Pressure Linked Equations.

Ansys Forte is a Computational Fluid Dynamics (CFD) software specifically intended to aid in the design of internal combustion engines through simulation. Its spray dynamics

and fuel combustion kinetics make it a formidable tool for simulating the mixing and combustion of liquid fuel with the entering air. To add further on this, Ansys Forte builds on models and sub-models that have been validated against experimental data over many years.

CFD is a numerical method used to model fluid flow. It is "the field of study concerned with analyzing various types of fluid flows with numerical simulations and developing suitable simulation algorithms" (Kajishima, Taira, 2017, p. 1). Now, the main advantage of CFD is "its ability to simulate flows in close to practical conditions–in terms of tackling real, three-dimensional, irregular flow geometries and phenomena involving complex physics" (Jayanti, 2018, p. 2), something which cannot be done using analytical solutions.

The equations describing fluid flow consist of conservation of mass, momentum, and energy, as well as equations of state that define the thermodynamic properties of the fluid. The governing equations are non-linear partial differential equations, making analytical solutions very hard to obtain and only possible in highly idealized conditions; rendering them impractical for real-world problems (Jayanti, 2018, p. 2).

Unlike in the air-standard analysis, in internal combustion engines, the mixture of air and fuel is the working fluid. Furthermore, due to the combustion of this liquid-gaseous mixture, reactions and phase changes take place; not to mention that the flow inside the cylinder is turbulent. To represent the fluid flow and its basic dynamics, Ansys Forte uses the Navier-Stokes equations. To model mass, momentum, and energy transport, conservation laws that represent the turbulent nature of the flow are formulated for the compressible gas-phase flows (Ansys Forte Theory Manual, 2022, p. 3).

The governing equations used in Ansys Forte are the species, fluid continuity, momentum conservation, energy conservation equations, and the gas-phase mixture equation of state. The species conservation equation models the gas-phase working fluids as a mixture of individual gas components whose composition changes during the engine cycle due to "flow convection, molecular diffusion, turbulent transport, interactions with fuel sprays, and combustion" (Ansys Forte Theory Manual, 2022, p. 4).

The fluid continuity equation is similar to the mass conservation equation used in fluid mechanics, although with some differences. The equation has the following form (Ansys Forte Theory Manual, 2022, p. 4):

$$\frac{\partial \bar{\rho}}{\partial t} + \nabla \cdot (\bar{\rho}\widetilde{\boldsymbol{u}}) = \dot{\bar{\rho}}^{s} \tag{4}$$

Here, $\bar{\rho}$ is the average density, $\dot{\bar{\rho}}^{s}$ is a source term due to spray evaporation (used in the species conservation equation), and $\widetilde{\boldsymbol{u}}$ is a Favre-averaged or density-weighted average velocity vector defined as (Ansys Forte Theory Manual, 2022, p. 3, 4):

$$\widetilde{\boldsymbol{u}} = \frac{\overline{\rho \boldsymbol{u}}}{\bar{\rho}} \tag{5}$$

The momentum conservation equation, "considers the effects of convection, pressure force, viscous stress, and turbulent transport, as well as the impact from liquid sprays and body force". The energy conservation equation is based on the first law of thermodynamics and is used to balance the change in internal energy due to pressure work and heat transfer. Also, the "effects of convection, turbulent transport, turbulent dissipation, sprays, chemical

reactions, and enthalpy diffusion of a multi-component flow" should be taken into consideration (Ansys Forte Theory Manual, 2022, p. 4, 5).

The gas-phase mixture equation of state is used to relate the thermodynamic properties of the fluid, such as pressure, temperature, density, and internal energy. The two equations of state that are supported in Ansys Forte are the ideal gas law and the real gas model. The ideal gas law is the simplest and the most used equation of state, as well as the default option in Ansys Forte. This equation has the following form (Ansys Forte Theory Manual, 2022, p. 5):

$$\bar{p} = R_u \bar{T} \sum_k \left(\frac{\bar{\rho}_k}{W_k} \right) \tag{6}$$

Where $\bar{p}$ is pressure, R_u the universal gas constant, $\bar{T}$ is temperature, $\bar{\rho}_k$ the density of species k, and W_k the molecular weight of species k. In Ansys Forte, the mixing of components is done according to the Dalton model (Ansys Forte Theory Manual, 2022, p. 5). When applying the Dalton model for gas mixtures, it is assumed that the gas mixture behaves as an ideal gas and the properties of each component of the mixture are considered to exist "separately and independently at the temperature and volume of the mixture" (Borgnakke, Sonntag, 2013, p. 516).

In summary, to derive the governing equations described earlier, Ansys Forte uses the gas-phase thermodynamic equation of state, Fick's law for mass diffusion, Fourier's law for thermal diffusion, and the assumption of a Newtonian fluid (Ansys Forte Theory Manual, 2022, p. 3).

In Ansys Forte, there are several ways to model the turbulence in internal combustion engines and they are essentially divided into two groups: the Reynolds-Averaged-Navier-Stokes (RANS) approach or the Large-eddy Simulation (LES) approach. The RANS approach simulates the ensemble average of the flow field, while the LES approach only simulates individual flow realizations. Using the RANS approach, a common practice is to model the turbulent transport processes with gradient-diffusion assumptions. In Ansys Forte, both the standard and advanced versions of the RNG (Re-Normalized Group) k-ε model are available, nevertheless, the recommended version is the advanced one (Ansys Forte Theory Manual, 2022, p. 3, 9 – 10).

When using the LES approach in Ansys Forte, the two options available are the Smagorinsky model and the dynamic structure model. The Smagorinsky model "is based on a viscosity assumption and accounts for the dissipative nature of turbulent flows, that is, kinetic energy is dissipated from the large-scale to the small-scale". On the other hand, the dynamic structure model is a non-viscosity and similarity-based model that relates the Sub-Grid-Scale (SGS) stress to the 'Leonard Stress'. In the end, the Smagorinsky model is recommended for its superior numerical stability when dealing with flows near complex boundaries (Ansys Forte Theory Manual, 2022, p. 12 – 13).

To make the simulation more realistic and relevant, the piston of a real gasoline engine was used. For this purpose, a piston from this engine was digitized to be used as part of our computational mesh in the software. The engine in question has the following specifications, some of which, will be input in Ansys Forte:

Table 1. Engine specifications.

Manufacturer	Volkswagen
Air intake	Turbocharged
Compression Ratio	10.5:1
Engine displacement (L)	1.5
Bore (mm)	74.5
Stroke (mm)	85.9
Connecting rod length (mm)	137
Number of cylinders	4

Just as in Ansys Forte, the rest of the chapter will be separated into subsections that follow the same order as the modeling nodes. Here, the information, parameters, and theory will be separated and explained accordingly. The nodes in order are geometry, mesh controls, models, boundary conditions, initial conditions, simulation controls, and output controls. After the output controls, a brief description of how the simulation was run will be included.

Geometry

To simulate the chosen internal combustion engine, a physical piston was digitalized using a GOM scanner. This allows for the obtention of data points that then form a data cloud. Then, this data cloud is later converted into a solid editable object in CATIA. The piston used is shown below:

Figure 10. The piston of the engine.

To scan the piston, it had to be painted using white opaque paint. This is because the metallic finish of the piston is shiny and may reflect the light of the scanner, causing errors when generating the geometry. Furthermore, stickers also had to be placed. These stickers serve as reference points for the scanner when generating the geometry. The prepared piston when scanning looks like this:

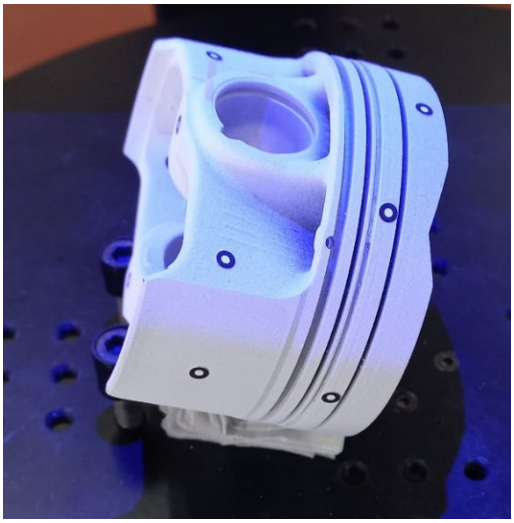

Figure 11. Prepared piston during scanning.

After scanning the piston, the data cloud was cleaned, and a section of the piston was then removed. Afterward, a mesh was created after polygonising and recalculating the generated cloud. This mesh was later exported as an STL file and imported into GOM Inspect. Here, all points were selected to close the mesh using a maximum hole size of 10 mm. Then, other holes had to be closed interactively. After all holes had been closed, the file was exported as an STL file again to finally convert it into a solid.

Now, since the only part of the piston relevant during combustion is the top surface, or the piston crown, the rest of the piston can be discarded. This means that from the region of the first compression ring to the bottom, including the zone where the second compression ring, oil ring, and wrist pin go, is eliminated.

However, an exact geometry of the piston is not necessary for performing the simulation. Since the piston has valve recesses and there will be no moving valves, as well as intake and exhaust ports, the piston can be approximated or idealized using only the piston bowl. From the STL file that was obtained, a profile was created in CATIA that best resembled the shape of the piston bowl. The piston had the following shape:

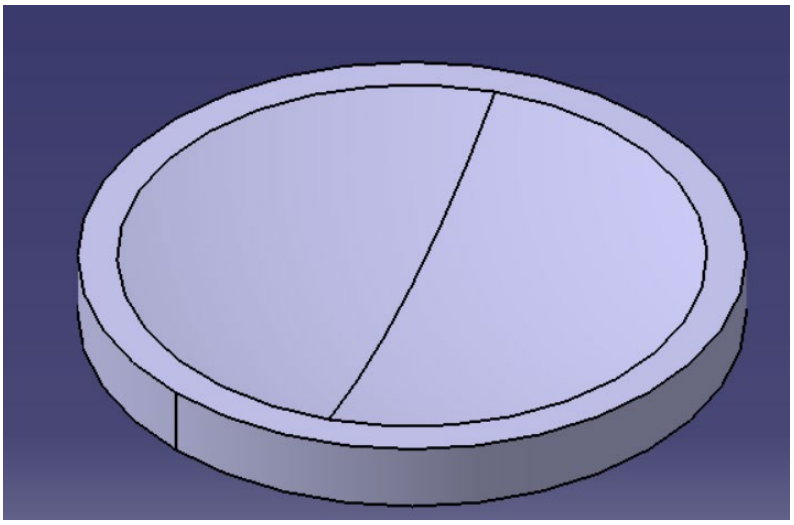

Figure 12. Piston bowl.

The radius of the groove operation performed on the piston was 32.57 mm, and the diameter and height of the piston were 73.85 mm and 7.7 mm. The lowest point in the groove operation is 4 mm below the upper surface of the piston.

Besides the piston, the cylinder liner and head had to be created. These are necessary to enclose the fluid and have a domain. So, the liner was made as a separate body having the shape of a thin ring with 0.15 mm of thickness starting from the top surface of the piston. To calculate this height, the main equation to be used is equation 1. But first, the volume of the head had to be calculated. To do this, a proposed height of 7 mm was used for the cylinder head since the dimensions of the cylinder head are not available.

Due to its dimensions and shape, the head has the shape of the half of an ellipsoid. The volume of the ellipsoid is calculated with the following equation:

$$V = \frac{4\pi}{3} abc \tag{7}$$

Where *a*, *b*, and *c* are the radii of the ellipsoid in the three directions; X, Y, and Z. In this case, *a*, *b*, and *c* were directly obtained from the geometry in CATIA, meaning that:

$$a = b = 36.925\ mm\ ;\ \ c = 7\ mm$$

Where a is the radius of the piston. With this information, the volume of half an ellipsoid corresponding to the head is calculated as follows:

$$V_H = \frac{4\pi}{6}abc = \frac{4\pi}{6}(36.925\ mm)^2(7\ mm) = 19989.30348\ mm^3$$

With the information from table 1, we can calculate the displacement volume V_h to then obtain the compression volume V_c. The displacement volume is calculated just as the volume of any cylinder:

$$V_h = \pi r^2 h \tag{8}$$

Where *r* is the radius of the engine cylinder (bore/2) and *h* is the stroke of the piston. Substituting these values in equation 7 gives a displacement volume per cylinder of 374451.514 mm^3. Then, we can use equation 1 to obtain an expression for V_C:

$$V_c = \frac{V_h}{\varepsilon - 1} \tag{9}$$

Using equation 8, it was found that the compression volume is equal to 39415.94884 mm^3. This is the total compression volume within the cylinder when the piston is at TDC, meaning that it includes the volume of the head plus the one occupied by the liner. To obtain the volume occupied by the liner, we need to subtract the head volume from the compression volume. Hence, this volume is:

$$V_L = V_c - V_H = 19426.64536\ mm^3$$

The subscript "L" means Liner. This now corresponds to the volume of a cylinder, meaning that the height of the liner h_L can now be obtained:

$$V_L = \pi r^2 h_L$$

$$h_L = \frac{V_L}{\pi r^2} = \frac{19426.64536\ mm^3}{\pi(37.25\ mm)^2} = 4.45651\ mm \approx 4.456\ mm$$

The cylinder head was also made as a separate body and no calculations were necessary, since it was made as half an ellipsoid starting from the top surface of the liner (Z = 12.156 mm from the absolute origin). The final geometry looks like this:

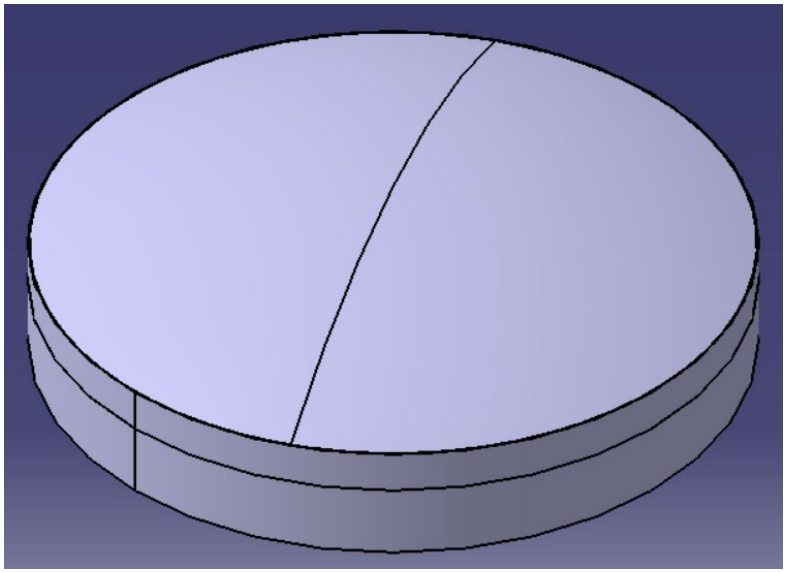

Figure 13. Piston, head, and liner geometries.

Before importing the geometry into Ansys Forte, a final step had to be done. A volume had to be extracted from the three bodies, to have a fluid domain that is bounded by the piston crown, head, and liner. The three bodies of the corresponding CATPart geometry file were imported into SpaceClaim. Here, the volume was extracted in three parts. The first volume

was extracted using the bottom surface of the head as a boundary and the outer surface of the head as the root surface, and later deleting the bottom surface to have the curved shape on top. The second volume was extracted by using the internal edges of the liner and its internal face to generate a disc, then the upper and lower surfaces were deleted to generate a ring. The third volume was extracted by using the piston crown surface as the root and the outer part of the piston as the boundary. Later, the extracted volumes were merged and the solid bodies were suppressed for physics. Finally, the volume was exported as a .tgf file, which is an Ansys Fluent meshing faceted geometry file. The extracted volume looked like this:

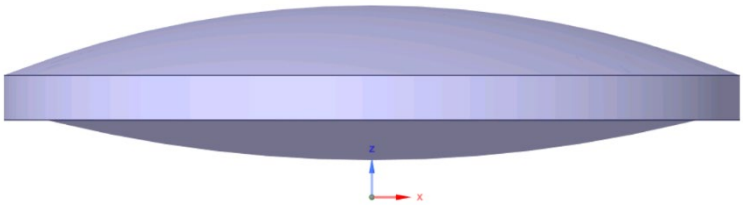

Figure 14. Extracted volume as seen from the XZ plane.

After importing the .tgf file using mm as units into Ansys Forte, some adjustments had to be made. The mesh had to be split three times to obtain the three surfaces. The first split used a point in the plane of 7.7 mm (thickness of the piston) in the Z direction (X = Y = 0), and a normal vector of Z = 4.456 mm (height of the liner). This is because the top surface of the piston crown is located in Z = 7.7 mm and the liner begins here.

Then, the second split used is Z = 12.156 mm as the point on the plane and Z = 7 mm (height of the head) as the normal vector. Now, there are three separate surfaces, the piston, the liner, and the head. As a final measure, the surface is checked for errors. No errors were

found after checking the surface mesh, meaning that we can now proceed with the rest of the simulation.

Mesh controls

One of the most important aspects of any CFD simulation is to have adequate mesh refinements and controls. The first step is to specify the location of the material point. This is a point that must always be inside the computational domain or enclosed by the boundaries. It also has to be at least one unit cell length away from the boundaries (Ansys User's Guide, 2022, p. 54). The coordinates used to locate the material point were X = Y = 0 and Z = 8.5 mm.

Then, a global mesh size was defined. As seen in many tutorials and Best Practices, the recommended global mesh size is 2 mm (Ansys Best Practices, 2022, p. 16), so this size was used. After these main settings for the mesh creation, some refinements were defined. These refinements were taken from the Best Practices and the tutorials.

The most important refinement is to apply a surface refinement to all boundaries using ½ of the global mesh size with 1 cell layer. This surface refinement is always active and is applied to the whole domain. The second refinement is another surface refinement that is only applied to the head, piston, and liner. Since in this simulation these are the only surfaces, then this mesh refinement is applied to all surfaces. Its size is ¼ of the global mesh size and has 2 cell layers. Unlike the previous surface refinement, this one is only active near TDC (squish region), meaning that it is active at 20° Crank Angle (CA) before and after TDC.

The next refinement corresponds to the spark plug. For this, a point refinement is used. This type of refinement consists of a sphere of influence where you can specify the minimum cell edge size relative to the global mesh size (Ansys User's Guide, 2022, p. 54). Here, the point refinement is located the same as the spark. For this a reference frame was created specifically for the spark plug with coordinates X = 3mm, Y = 0, Z = 19.111 mm, and a rotation about the Y axis of 185°, effectively making the Z axis of this new reference frame point downwards. Using this reference frame, a value of Z = 0.5 mm was set, with X = Y = 0. The radius of application of the sphere is 0.6 cm and here, the mesh size will have a fraction of 1/8 of the global mesh size. Furthermore, it is active at 25° CA before and after TDC.

The last mesh refinements correspond to two types of Solution Adaptive Meshing (SAM) strategies. This allows meshing based on a solution field (or gradient) at the current time step. Cells are refined and/or coarsened according to the criteria specified by the user. Normally, these meshing strategies are almost always applied to gradients, and here, the statistical bounds are very useful. All of the SAM strategies used in this simulation are specified as a gradient of the solution field unless described otherwise (Ansys User's Guide, 2022, p. 56).

The first SAM is applied to the velocity magnitude to resolve flow fields (Ansys Best Practices, 2022, p. 18). This refinement uses ½ of the global mesh size and a statistical bound with a sigma threshold of 0.5. Recommended values of sigma range from 0.5 to 1; a lower value of sigma leads to more refinement, while a higher value leads to less refinement. This SAM is applied to the entire domain and is active always.

The second SAM is applied to the temperature to resolve reacting regions (Ansys Best Practices, 2022, p. 19). This refinement uses ¼ of the global mesh size and statistical bounds with a sigma threshold of 0.5. It is applied to the entire domain but it is only active from 20° CA before TDC to 80° CA after TDC. This concludes the mesh refinement settings for the simulation.

Models

The first and most important model to be used in the simulation is the chemistry model. Ansys Forte has several chemical sets that, depending on the application, include hundreds of species that participate in thousands of reactions. The chemistry model is responsible for all the chemical processes and chemical kinetics involved in combustion, as well as the species involved.

In this work two simulations will be done, one with only gasoline to generate the baseline data for the comparison and one using E10. Hence, a different chemistry set has to be selected per simulation. In the case of only gasoline (E0), the corresponding chemistry set is *Gasoline_1comp_49sp.cks*; while for the simulation with E10, the chemistry set is *Gasoline-ethanol_4comp_179sp__soot-pseudo-gas.cks*. The pseudo gas chemistry set was chosen because the soot particle number and size will not be needed (Ansys User's Guide, 2022, p. 253).

Following the recommendations seen in the Best Practices documentation (Ansys Forte Best Practices, 2022, p. 22), the last step after importing the chemistry set is to include a flame library that includes the fuel components to be used in the simulation under direct injection conditions. Two flame speed libraries will be created, one for each simulation. In

the simulation using gasoline, the flame library will only consist of iso-octane (ic8h18 in Ansys Forte) as the species. To model gasoline, iso-octane is used as the species and this species serves as a surrogate for the fuel. In the simulation using E10, the flame library must contain iso-octane and ethanol (c2h5oh). The flame speed model values are left at their defaults.

The equation of state to be used in the simulations is the ideal gas law, not only because it is the default option, but because of the operating conditions that meet the criteria for its use. These criteria specify that the temperature of the gas has to be greater than the critical, and the pressure lower than the critical to use the ideal gas formulation. These temperatures and pressures will be shown later in the initial conditions section.

The values of the transport model are also left at their default values since there is no need to adjust them. Also, the RANS RNG k-ε model will be used as a default, since it is recommended as the best model for engine flow and combustion problems (Ansys Forte Best Practices, 2022, p. 21). This model is recommended over the standard version because the ε equation in the RNG version is based on rigorous mathematical derivation instead of empirically derived constants. Furthermore, the ε equation has one additional term that accounts for anisotropic turbulence (Ansys Forte Theory Manual, 2022, p. 10 – 11).

When activating the spark ignition model, the flame propagation model presents the first options available for the edition. The only inputs to be modified here are the kernel flame to G-equation switch constant, with a value of 2.0, and the flame development coefficient, with a value of 0.5. A typical value of the kernel flame to G-equation switch constant is 2.0, as described in the theory manual (Ansys Forte Theory Manual, 2022, p. 70). This constant

controls the transition from the ignition kernel (starting point of combustion) to the G-equation model. Such transition occurs only when the kernel radius grows larger than the product of this coefficient times the turbulence integral length scale. On the other hand, the flame development coefficient controls the "exponentially increasing effect of turbulence on flame propagation speed as the flame grows from laminar to fully developed turbulent flame" (Ansys Forte User's Guide, 2022, p. 76).

Very briefly, the G-equation model is used to describe turbulent combustion since it is based on the turbulent premixed combustion flamelet theory developed by Norbert Peters. This model consists of Favre-averaged level-set equations that include the equations for the Favre mean, its variance, and a model equation for the turbulent/laminar flame surface area ratio. These equations along with the RANS and turbulence modeling equations describe the premixed turbulent flame-front propagation (Ansys Forte Theory Manual, 2022, p. 71).

The next step is to create a spark by first specifying its location. The location was set using the previously created reference frame for the spark plug. Using this reference frame, a value of Z = 0.5 mm was set, with X = Y = 0. Next, is the timing option. In this case, we will use the same timing option as in tutorial 7, by specifying the start of ignition at 15° CA before TDC with a typical duration of 10° CA as specified in the Best Practices. The final settings in the spark plug refer to the spark energy. Following the recommendations seen in Best Practices, the energy release rate is set to 20 J/s, the energy transfer efficiency to 0.5, and the initial kernel radius to 0.5 mm (Ansys Forte Best Practices, 2022, p. 26).

Boundary conditions

The next step in the simulations is to assign boundaries to each of the surfaces that enclose our volume or fluid domain. In this case, all boundaries correspond to a wall boundary with a thermal boundary condition. Only the temperatures will be modified and all other parameters are left at their default values, except for the piston. As a consequence, the Law of the Wall is the option used for the wall-boundary layer model. In the following settings and some of the initial conditions, we start from the data seen in the 5th tutorial by Ansys Forte.

For the Head and Liner geometries, a constant wall temperature of 385 K was applied, while for the piston, a temperature of 420 K was applied (Ansys Forte Tutorials, 2022, p. 49 – 50). Besides the temperature, the wall motion with a slider-crank type was used for the piston. Here, a stroke of 8.59 cm and a connecting rod length of 13.7 cm were input with a piston offset of 0.

In the tutorials or case studies done, these wall temperatures are between 385 K and 500 K. Because combustion begins at the top of the cylinder, the hottest parts will be the top surface of the piston, liner, and the bottom part of the head. In an internal combustion engine, even when temperatures may reach up to 2500 K, the hot exhaust gas never resides too much inside the cylinder. Shortly after combustion it is expelled and later, fresher cooler air is drawn in through the intake valve. Because of this, there is barely any time for heat transfer to occur between the hot exhaust gas and the cylinder walls.

Also, when performing the air-standard analysis of the Otto cycle, the boundary temperatures are between the ambient temperature ($T_1 \approx 300$ K) and the temperature at which

the piston has fully compressed the air at TDC ($T_2 \approx 680$ K). That is why these wall temperatures serve as an adequate approximation for the thermal boundary conditions. Nevertheless, it is proposed as a future work to use temperatures closer to the ones obtained experimentally by other authors.

Initial conditions

Each region in Ansys Forte requires the specification of initial temperature, pressure, and species. Other additional components such as turbulence or velocity may be specified. The first input is the composition. In the case of in-cylinder engine simulations only, the composition to be specified corresponds to the gaseous mixture trapped inside the cylinder when the intake valve has closed (IVC). This composition can vary according to how the simulation is set, in some cases, it is only air or exhaust gas.

Since the simulation will begin after IVC, and injection timing, as well as injection duration of the engine, are unknown, it is proposed that injection occurs during the intake valve lift at the intake stroke; meaning that by the time our simulation begins, the fuel will have already vaporized and mixed with the air. Using this assumption, a gaseous composition for the initialization region was created using the composition calculator of Ansys Forte. Here, the fuel mass for each simulation and composition were specified.

For both simulations, a fuel mass of 30 mg – slightly higher than the one used in tutorial 7 (27 mg) – is used. For the simulation of gasoline, the fuel composition was defined using iso-octane as the species (fuel surrogate) with a mass fraction of 1. Then, for both simulations standard air is used as well as no EGR (Exhaust-Gas-Recirculation), and air flow is left at its default values. To calculate the mixture, the option is selected as premixed after

injection. With these settings, a gaseous composition of the fuel being vaporized and premixed with air is created, meaning that this is now an ignitable mixture.

For the simulation with E10, the fuel composition uses the densities of gasoline and ethanol to calculate the mass fraction in the fuel. The density values were taken from the data provided by Iliev (2021, p. 2). Here, he specifies that gasoline and ethanol have a density of 740 kg/m^3 (0.74 g/cm^3) and 785 kg/m^3 (0.785 g/cm^3) respectively. Knowing that E10 is 10% ethanol and 90% gasoline by volume, then in 1 L of E10 there are 100 cm^3 of ethanol and 900 cm^3 of gasoline. With this information, it is possible to obtain the mass fraction of ethanol and gasoline in E10:

$$m_E = \rho_E V_E = \left(0.785 \frac{g}{cm^3}\right)(100\ cm^3) = 78.5\ g$$

$$m_g = \rho_g V_g = \left(0.74 \frac{g}{cm^3}\right)(900\ cm^3) = 666\ g$$

The total mass of E10 is $m_T = 744.5\ g$. With the total mass and the mass of each component, it is possible to obtain the mass fraction and then create the E10 fuel composition in Ansys Forte:

$$m_{FE} = \frac{m_E}{m_T} = \frac{78.5}{744.5} = \frac{157}{1489} \approx 0.10544$$

$$m_{Fg} = \frac{m_g}{m_T} = \frac{666}{744.5} = \frac{1332}{1489} \approx 0.89456$$

These values were then input into the mixture editor in Ansys Forte, using 0.10544 as the mass fraction for the species known as ethanol (C_2H_5OH) and 0.89456 for iso-octane (iC_8H_{18}).

After specifying the composition, the next parameters are the initial temperature and pressure of this gaseous mixture. These were obtained after running the 5th tutorial with gasoline and E10 from 1000 to 6000 RPM with increments of 500 RPM and using a stroke that gave a similar compression ratio to the one used in our simulations (10.5).

The 5th tutorial of Ansys Forte consists of a port-fuel spark-ignition engine. This tutorial has intake and exhaust manifolds, as well as their respective valves. In this engine, fuel is premixed in the intake manifold to later enter a cylinder with a gaseous composition of exhaust gas. So, the data needed from this tutorial are mainly the temperatures and pressures at IVC for our simulations, as well as the final results to corroborate that our simulations are indeed correct or at least within the expected values. It is important to mention that the pressures presented in the following tables correspond to a naturally aspirated engine. Since the boost pressures of the turbocharger are unknown, the engine will be simulated as if it were naturally aspirated. With this having been said, a table of initial temperature and pressure depending on RPMs is presented for each fuel:

Table 2. Initial temperatures and pressures for the simulation running with gasoline

RPM	**Temperature (K)**	**Pressure (MPa)**
1000	475.1	0.2754
1500	473.56	0.2842
2000	475.13	0.2942
2500	467.2	0.286
3000	475.36	0.3037
3500	470.22	0.2911
4000	470.78	0.2991

4500	480.5	0.3282
5000	492.46	0.3648
5500	501.82	0.3963
6000	507.95	0.4175

Table 3. Initial temperatures and pressures for the simulation running with E10

RPM	**Temperature (K)**	**Pressure (MPa)**
1000	475.32	0.2756
1500	472	0.2826
2000	475.22	0.2943
2500	467.27	0.2862
3000	475.64	0.304
3500	470.38	0.2911
4000	470.95	0.2992
4500	481.56	0.3311
5000	491.85	0.3624
5500	501.94	0.3966
6000	507.78	0.4166

After specifying the initial temperatures and pressures, the next parameter is turbulence. This indicates how the fuel is mixed in the cylinder. For both simulations, a turbulent kinetic energy of 7900 cm^2/s^2 and a turbulent length scale of 0.4 cm is set, just as in tutorial 5. The turbulent length scale serves as the boundary value for epsilon in the k-ε turbulence model (Ansys Forte User´s Guide, 2022, p. 87).

The last settings under the initial conditions node correspond to how velocity is initialized. Within the cylinder, the air drawn in from the intake valve generates a turbulent rotational flow, causing the air to adopt a swirl pattern. Swirl is very important for turbulent mixing and combustion efficiency in engines, and for this reason, velocity is initialized using engine swirl in both simulations.

Just as in the 5th tutorial, the initial swirl ratio is set with a factor of -0.0739. The initial swirl ratio is defined as the air rotation rate to the crankshaft rotation rate. A positive value indicates counterclockwise motion and a negative value indicates clockwise motion when viewed from the positive Z direction.

Another important parameter when setting the engine swirl is the initial swirl profile factor, which is a "dimensionless constant that defines the initial azimuthal velocity profile". For all simulations, the recommended and default value of 3.11 will be used (Ansys Forte Theory Manual, 2022, p. 27 – 28).

After setting the engine swirl, the "Initialize Velocity Components Normal to Piston" option is activated. By activating this option, the axial velocity of the piston is set to be equal to the piston velocity at the piston surface (Ansys Forte User's Guide, 2022, p. 104). Finally, the piston boundary for which this velocity is initialized must be selected.

Simulation controls

If the geometry for intake and exhaust manifolds is available, as well as their respective valves, it is typical to start and end the simulation in crank angles that include the opening and closing of the intake and exhaust valves. However, for in-cylinder-only simulations, just

as in this present work, the initial crank angle corresponds to when the intake valve is closed (IVC) and the final crank angle corresponds to when the exhaust valve opens (EVO) (Ansys Forte Best Practices, 2022, p. 11).

However, it is important to consider a convention for crank angles. The crank angle where the piston is at the TDC of the compression stroke corresponds to CA = 0°, and precisely, Ansys Forte uses the same convention. For automatic mesh generation cases, TDC corresponds to CA = 0° (Ansys Forte User's Guide, 2022, p. 93). In a simplified way, this means that 0 – 180° CA is the power stroke (expansion), 180 – 360° CA is the exhaust, 360 – 540° CA is the intake, and 540 – 720° CA is the compression.

For this simulation, the initial crank angle corresponds to IVC, which according to our engine is -60° CA or 660° CA. Hence, the simulation will begin during the compression stroke. The final simulation crank angle corresponds to EVO, which is approximately 140° CA or 860° CA. Both simulations will be run from 1000 to 6000 RPM (redline) in increments of 500 RPM. The last parameter to be input is the engine bore, which is user-specified and corresponds to the value seen in Table 1.

For the time step options, an initial simulation time step of 5E-6 sec. will be used. The time step will also be restricted by a max. CA delta per time step of 1.1. Furthermore, the max. simulation time step has a constant value of 1E-5 sec. The advanced time step control options will be left at their default values.

For the chemistry solver, the absolute and relative tolerance values will be left at their defaults, which are 1E-12 and 1E-5 respectively. Dynamic Cell Clustering (DCC) is activated

and left with its default values. The DCC method groups computational cells of high similarity into clusters, making it more efficient and requiring a solution of the kinetic equations only once for each cluster. This algorithm only requires the max. temperature dispersion (10 K) and max. dispersion in equivalence ratio (0.05) as inputs (Ansys Forte Theory Manual, 2022, p. 36). The transport terms need no modification and all are left at their defaults.

Output controls

In the output controls node, there are two options available, spatially resolved and spatially averaged species. For the spatially resolved species, an interval-based output of 20° CA is set. Additionally, a user-defined crank angle output is set from the start of ignition to the end of ignition, going in 2° CA increments. This is done to manage the size of the results file when Ansys performs the simulation The spatially resolved species are all of those relevant to combustion and emissions, these include N_2, O_2, CO_2, H_2O, CO, NO, NO_2, iC_8H_{18}, C_2H_5OH, and OH.

For the spatially averaged species, the output is set to every 1° CA. Here, the results are written into CSV files, which is not a problem in terms of hard drive space. The spatially averaged species are all of those relevant to combustion, these are the species already mentioned above.

The last setting in the output controls node is the restart data. This is useful if unexpected problems during the simulation occur and for some reason, the simulation is interrupted, causing the simulation to fail. As a countermeasure, restart files serve as checkpoints for the simulation to take off from the last saved crank angle or cycle, instead of

starting from the very beginning. For this reason, the “Write restart file at last simulation step” option is checked and a profile for user-defined restart points is set in increments of 30° CA.

Running the simulation

The simulation was performed doing parallel runs using a total of 8 MPI arguments. As a guideline, one parallel run with 4 MPI arguments at 1000 RPM took 8 hours and 34 minutes to complete using a computer with 31.6 GB of usable RAM and on 8 cores of an Intel(R) Xeon(R) processor W-2145 CPU at 3.70 GHz.

Chapter 3

In this final chapter, the results of the performance and emissions of the engine using gasoline and E10 will be discussed. An extensive analysis of both will be done to further understand the why of these results.

Performance results and discussion

The results obtained with E10 compared to gasoline coincide and agree with the literature. Not by any exact percentage or amount, but by the relative differences between them. The general trend shown in terms of performance by E10 is that it is slightly lower than gasoline's. The following figure shows the gross indicated power curves for gasoline and ethanol as a function of RPM:

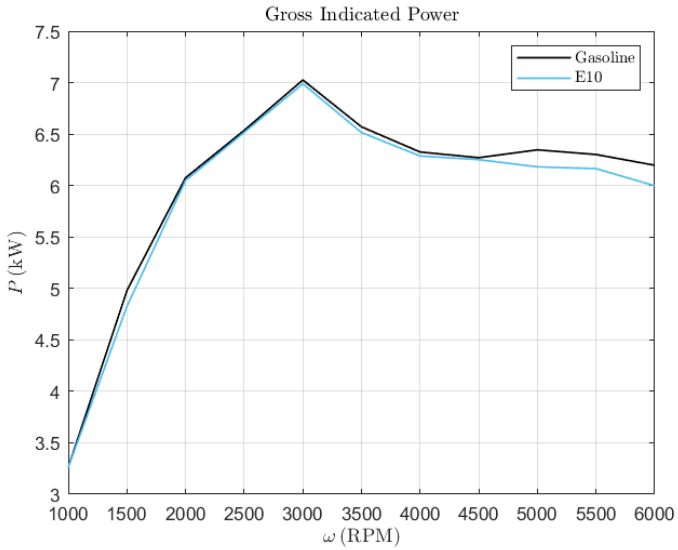

Figure 15. Gross indicated power for gasoline and E10 as a function of RPM.

From Figure 15 it can be seen that gasoline and E10 are very evenly matched in terms of power output, with the maximum power output registered at 3000 RPM for both fuels, 7.02593 and 6.98873 kW for gasoline and E10 respectively. Even adding a small amount of

ethanol to gasoline, lowers the total calorific value of the fuel. This can be seen more properly from 4500 RPM and beyond, where the difference in power becomes greater. The biggest difference in power output is found at 6000 RPM, where E10 produces 3.22% less power than gasoline. Given the lower calorific value of ethanol and the fact that at high RPM the combustion time and airflow in the cylinder are lower, it is possible that at high RPM there is a greater difference in terms of power between both fuels. On average, E10 produced 1.28% less power than gasoline throughout the entire speed range.

As predicted by the literature, power output using E10 is lower because of the lower calorific value of ethanol. At 5000 RPM, E10 gave 2.60% less power than gasoline, which is similar to the results obtained by Tibaquirá *et al* (2018, p. 6 – 7). They obtained negligible power losses at 5000 RPM when using E10. Moreover, these results coincide with those of Iliev in both of his works (2015, p. 93), (2021, p. 8). He found that engine power decreased for E10 when compared to gasoline at all engine speeds (1000 – 6500 RPM), also by a very small amount. Finally, this also concurs with the research done by Dhande *et al* (2021, p. 303), where they found that engine power using E10 was lower than gasoline from 1300 to 1800 RPM.

As a consequence of a higher power output with gasoline, torque will also be higher. Although this value is not directly provided by the software, it can be calculated using equation 3, presented at the beginning of chapter 1:

$$T = \frac{P}{\omega}\ [Nm]$$

With this information, it is possible to obtain the torque curves using gasoline and E10:

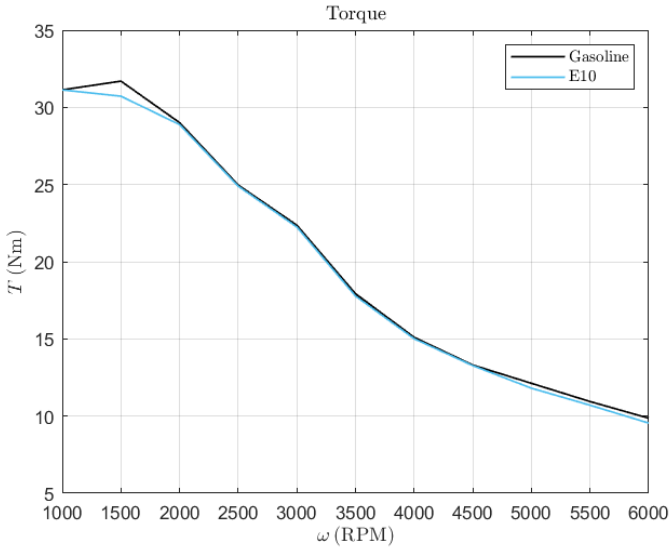

Figure 16. Torque curves for gasoline and E10 as a function of RPM.

From these torque results, it can be seen that gasoline produces the highest torque at 1500 RPM, and the biggest differences about E10 are seen here and at 6000 RPM. At 1500 RPM, torque using E10 is 3.08% lower than gasoline, while at 6000 RPM E10 has a torque deficit to gasoline of 3.22%. In general, the differences in torque throughout the whole speed range, are very small. At 5000 RPM, Tibaquirá *et al* (2018, p. 7) reports having a negligible loss of torque when using E20, but E10 produced more torque than E20, so this loss is even smaller. Iliev (2015, p. 93) also had very similar results, a barely perceptible loss of torque when using E10. This correlates with the lower engine output produced by E10 as a consequence of a lower calorific value of the blend. On average, E10 produced 1.28% less torque than gasoline throughout the entire speed range.

The next performance value is the Indicated Mean Effective Pressure (IMEP). This is another parameter that reflects engine performance because it is directly related to the work done by the piston during the compression and expansion strokes. It is important to mention that the simulation begins during the compression stroke (60° before TDC) and ends during the expansion or power stroke (140° after TDC). This only covers 200° of crankshaft movement, 160° less than half of a cycle (360°).

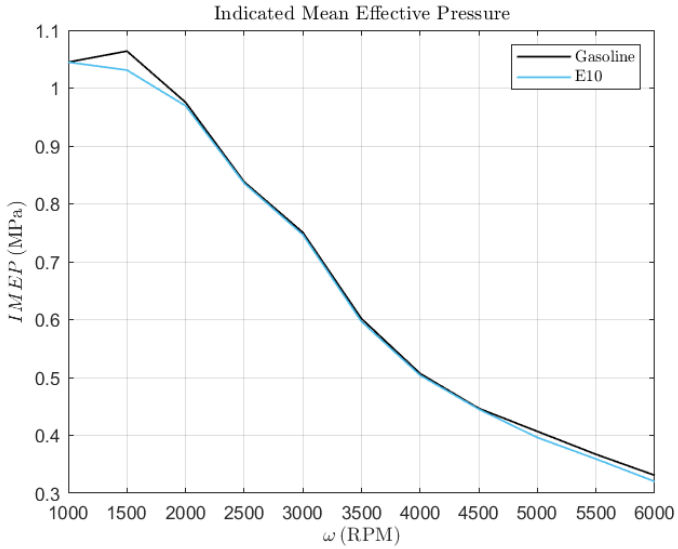

Figure 17. Indicated Mean Effective Pressure for gasoline and E10 as a function of RPM.

Once again, the trend is the same, with E10 having lower IMEP values than gasoline but only by a little. The biggest difference is observed at 1500 RPM, with gasoline producing an IMEP 3.17% higher than E10. The results here, however, do not coincide at all with those of the literature. From 2400 to 2700 RPM, Yusuf and Inambao (2021, p. 888) report that E10 had a higher IMEP. Rosdi *et al* (2020, p. 5) show that E10 had a higher IMEP at 40% Wide Open Throttle (WOT) and 3000 RPM. Likewise, Elshenawy *et al* (2023, p. 6) report an increase of 4.1% in IMEP for E10 at 2500 RPM; while the results achieved through these

simulations indicate a loss of 0.302% in IMEP for E10 against gasoline at the same speed. On average, E10 had an IMEP 1.3% lower than gasoline throughout the entire speed range.

Next, is the gross Indicated Specific Fuel Consumption (ISFC). This is the only parameter in which E10 has higher results than gasoline, which is undesirable because a higher fuel consumption leads to higher emission levels and expenditures for refueling the vehicle. However, despite this higher fuel consumption, many emissions produced by E10 are less than with gasoline, as will be seen later. But for now, the following figure illustrates the gross ISFC as a function of RPM:

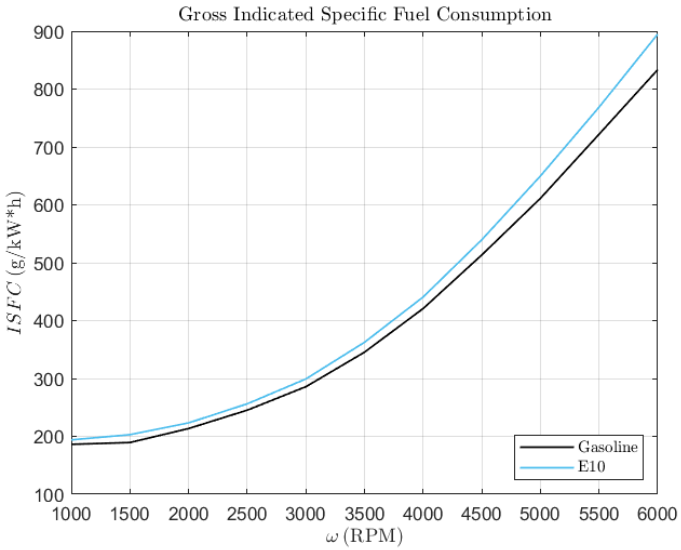

Figure 18. Gross Indicated Specific Fuel Consumption for gasoline and E10 as a function of RPM.

The lower calorific value of ethanol and its blends with gasoline leads to greater fuel consumption because more fuel is needed to maintain the same power output. This is confirmed by the results found by Pham *et al* (2015, p. 7), who found that fuel consumption increased with E10 in their experiments made with the fuel-injected car, in a vehicle speed

from 45 to 75 km/h at 4th gear, and Tibaquirá *et al* (2018, p. 8), who simply states that ISFC increases with increasing ethanol content.

Even after consuming more fuel, it simply is not possible to produce the same or a greater power output compared to gasoline because of this limiting chemical property. Other authors have reached similar results. Dhande *et al* (2021, p. 303), affirm that ISFC increases with engine speed and ethanol content. This is confirmed by Iliev (2021, p. 8) and Rosdi *et al* (2020, p. 6). In their experiments, Dhande *et al* (2021, p. 303) found that E10 has an ISFC 12.12% higher than gasoline at 1600 RPM, while Elshenawy *et al* (2023, p. 6) found an increase in ISFC of 3.7% when using ethanol at 2500 RPM. In this present work, ISFC with E10 increased 7.16% at 1500 RPM, and 4.48% at 2500 RPM. On average, E10 had an ISFC 5.45% higher than gasoline throughout the entire speed range.

The final and one of the most important performance parameters in internal combustion engine design is thermal efficiency. This indicates how much of the fuel being burned is converted into useful mechanical energy that can power the vehicle. The results are shown below:

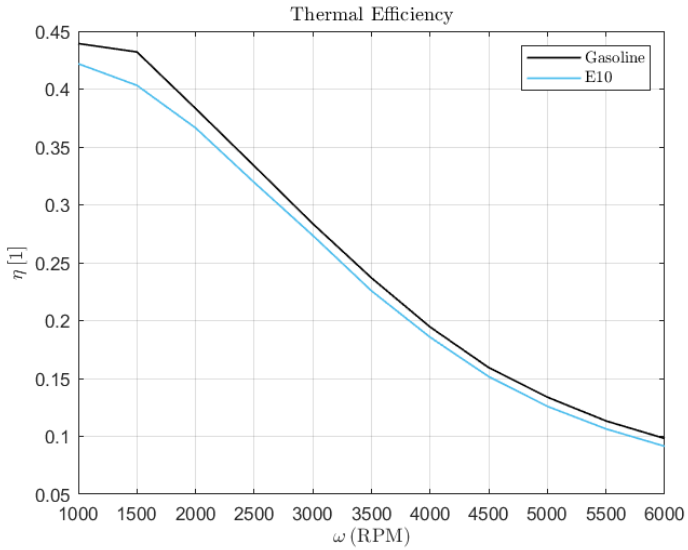

Figure 19. Thermal efficiency for gasoline and E10 as a function of RPM.

At all times, thermal efficiency is greater with gasoline than with E10, with the most likely reason being the lower calorific value of E10 compared to gasoline. The biggest losses in thermal efficiency are found at 1500, 5500, and 6000 RPM, with E10 having a decrease of 6.68%, 6.08%, and 6.86% at these speeds respectively, compared to gasoline.

From what is observed in Figure 19, thermal efficiency decreases with engine speed. This is because at higher engine speeds there are more frictional and thermal losses in the engine. Also, Dhande *et al* (2021, p. 302 – 303) found that thermal efficiency decreases with ethanol content and engine speed and that a possible cause may be incomplete combustion. This correlates very well with the higher emissions of unburnt hydrocarbons at higher speeds. Furthermore, Elshenawy *et al* (2023, p. 7) show that thermal efficiency is on average lower with increasing ethanol content and engine speed. Peak thermal efficiency is reached at 2300 RPM and then drops. In this present work, the highest values for gasoline and E10 were reported at 1000 RPM. Tibaquirá *et al* (2018, p. 8) also found lower thermal efficiencies

when using E10. On average, E10 had a thermal efficiency 5.08% lower than gasoline throughout the entire speed range.

Emissions results and discussion

The general trend in terms of emissions is that at no time a steady state is reached above 4000 RPM, both in gasoline and in E10; but at low revolutions it is. By 'steady-state' we mean that the curve is 'flattening' or already has very little variation, the curves neither continue to increase nor to decrease.

In the CO, CO_2, and $EINO_x$ (Emissions Index of NO_x) emissions results, a decreasing trend was found for both fuels as engine speed increased. For this reason, the figures of emissions as a function of crank angle presented here will not include the intermediate values, i.e., engine speeds of 1500, 2500, 3500, 4500, and 5500 RPM will not be shown. Nevertheless, an analysis at these speeds will be conducted. The Unburnt Hydrocarbons (UHC) and Volatile Organic Compounds (VOC) emissions results show an opposite trend, where these increase with engine speed. These emissions results also do not include intermediate values.

It is important to consider that in the figures of emissions as a function of crank angle (CA), the region from -60 ° CA to -15 ° CA combustion has not occurred and that is why emissions are 0 (except in UHC and VOC emissions). From -15° CA onwards, emissions start to rise as the spark ignites the air/fuel mixture. From -60° CA to 0° CA, the piston is compressing the air/fuel mixture in the cylinder, and from 0° CA to the end of the simulation the volume inside the cylinder is expanding because of the downward movement of the piston. The schematic below illustrates these positions:

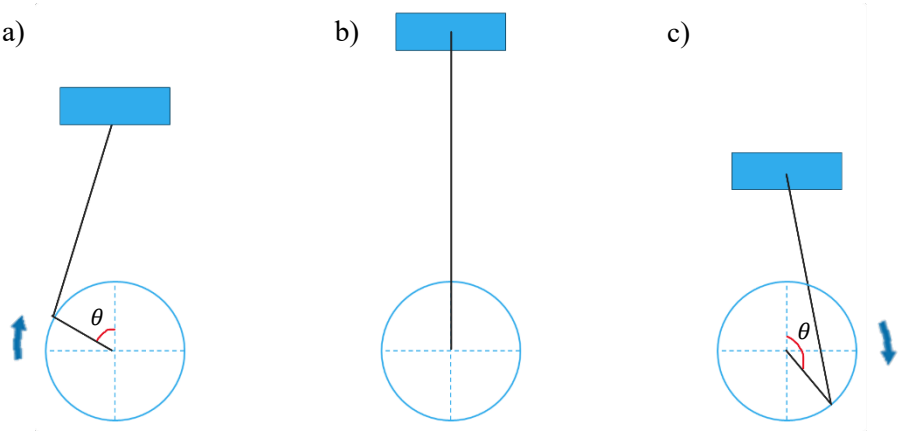

Figure 20. Schematic of the crank angle positions for: a) initial crank angle, b) TDC, and c) final crank angle.

Now, the following figure of CO emissions from 1000 to 6000 RPM for gasoline and E10 as a function of crank angle (CA) is shown below. However, it is important to mention that the continuous line represents the results for gasoline and the dotted line for E10. This is used for all the figures of this nature (emissions vs. crank angle).

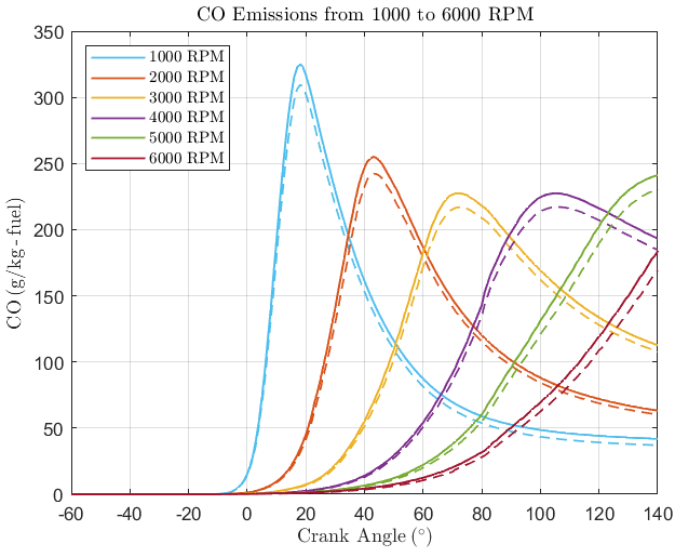

Figure 21. CO emissions of gasoline (–) and E10 (- - -) from 1000 to 6000 RPM.

From what can be seen in the previous figure, the peak in CO emissions registered after ignition for E10 is considerably lower than gasoline from 1000 to 2000 RPM and at all RPMs shown, the emissions at Exhaust Valve Opening (EVO) are lower. Peak CO emissions

were 4.8%, 6.4%, and 5.01% lower for E10 at 1000, 1500, and 2000 RPM respectively when compared to gasoline.

Also, when engine speed increases even more the peak cannot be seen and only a steep increase several crank angles after ignition can be appreciated. Even up to 4000 RPM the peak in emissions can yet be seen but not as clear as when the engine speed was 3000 RPM or lower. From 5000 RPM, only an increasing slope appears.

Now, when comparing the emissions of CO for both fuels from 1000 to 3000 RPM, and from 4000 to 6000 RPM, what can be noticed is that in the lower speed range, the peak in emissions is much higher but the emissions at EVO are much lower. The exact opposite occurs at the higher speed range, the peak in emissions is lower but at EVO these are much higher for both fuels. The key takeaway from these curves is that CO emissions for E10 are at all times lower than gasoline. This is a pattern that repeats for almost every pollutant, except the Volatile Organic Compounds (VOC) emissions.

From Figure 21, it can be seen that the peak in emissions is further delayed as the engine RPMs increase. The peak is dramatically shifted forward when comparing the emissions results seen at 1000 RPM to those at 3000 RPM. Furthermore, the peak of emissions is lower as engine speed increases. This behavior is also present in the emissions of CO_2, and the Emissions Index of NO_x ($EINO_x$).

For this reason and the different behavior of the emissions curves after certain RPMs, the emissions values that will be shown in the bar graphs for every pollutant are the ones

corresponding to when the exhaust valve opens (EVO), that is, at the end of the simulation. The following figure shows the results of CO emissions at EVO:

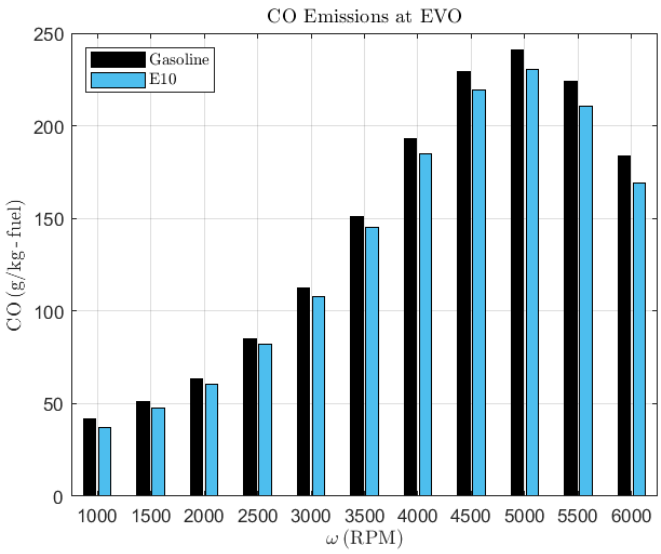

Figure 22. CO emissions at EVO for gasoline and E10.

From Figure 22, it can be seen that indeed CO emissions for E10 are lower throughout the entire speed range, with the smallest reduction in emissions seen at 2500 RPM. E10 produced 3.58% less emissions at this speed than gasoline, while the biggest reduction was seen at 1000 RPM, with E10 producing 11.6% less emissions than gasoline. The average CO emissions reduction throughout the entire speed range was 5.62%

Despite this, CO emissions increased with engine speed. This is because at higher speeds there is less time for fuel to burn completely and incomplete combustion occurs. And recalling what was seen in Chapter 1, CO emissions are a product of incomplete combustion.

The results obtained with these simulations agree very well with the literature revised, in the sense that CO emissions using ethanol blends are lower because of the more complete combustion achieved with them. Pham *et al* (2015, p. 7) obtained a reduction of 7.76% in

CO emissions when using E10. Wang, *et al* (2015, p. 152) only affirm that blended fuels promote more complete combustion that reduces these emissions. Iliev found that when increasing the ethanol content, CO emissions decrease because of the oxygen present in ethanol (2021, p. 10). Yusaf *et al* (2009, p. 4) found that CO emissions decreased at 3000 RPM by 24.31% when using E10, and Hosseini *et al* (2023, p. 12) that CO emissions decreased by 15.21% at this same speed but at full load with E10. In this work, only a reduction of 4.19% was achieved at 3000 RPM.

Now, Ansys Forte does not calculate the CO_2 emissions after combustion. However, these can be calculated with the following chemical reaction if complete combustion is assumed (Pulkrabek, 1997, p. 285):

$$CO + \frac{1}{2}O_2 \rightarrow CO_2 + \Delta \tag{10}$$

With this reaction, it is possible to obtain an estimate of the CO_2 emissions by using the ratio of the molecular weights between CO and CO_2. CO has a molecular weight of 28 g/mol and CO_2 has a molecular weight of 44 g/mol. By assuming complete combustion, something which Ansys Forte already does (Ansys Forte User's Guide, 2022, p. 24), it is possible to use the ratio of molecular weights to estimate the CO_2 emissions from the CO emissions. To do so, the CO emissions have to be multiplied by a factor of $44/28 \approx 1.5714$. Now the estimated emissions of CO_2 for gasoline and E10 as a function of CA from 1000 to 6000 RPM are shown below, where the continuous line represents the results for gasoline and the dotted line for E10.

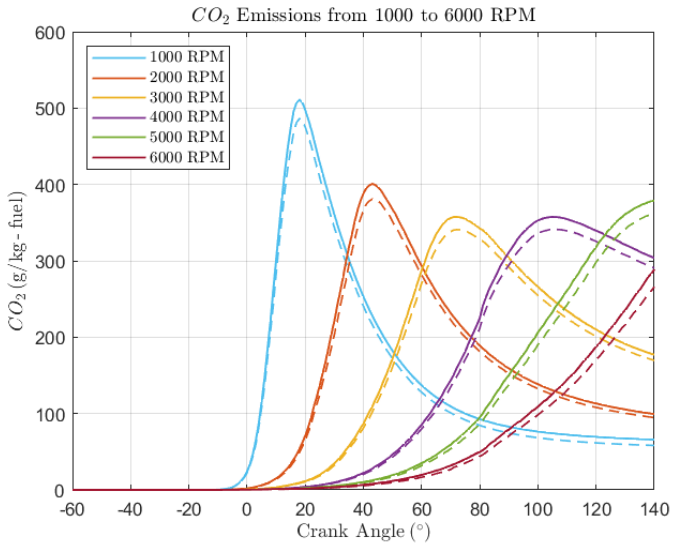

Figure 23. CO_2 emissions of gasoline (–) and E10 (- - -) from 1000 to 6000 RPM.

Now, since the CO emissions are multiplied by a factor of 44/28, the percentage difference in CO_2 emissions between gasoline and E10 remains the same as for CO emissions at all RPMs, as well as their behavior. From Figure 23, it can be seen that E10 has lower emissions than gasoline at the peak and at EVO. Moreover, the peak is greater in the lower speed range (1000 – 3000 RPM) with lower emissions at EVO, but conversely at the higher speed range. The following figure shows the results of CO_2 emissions at EVO:

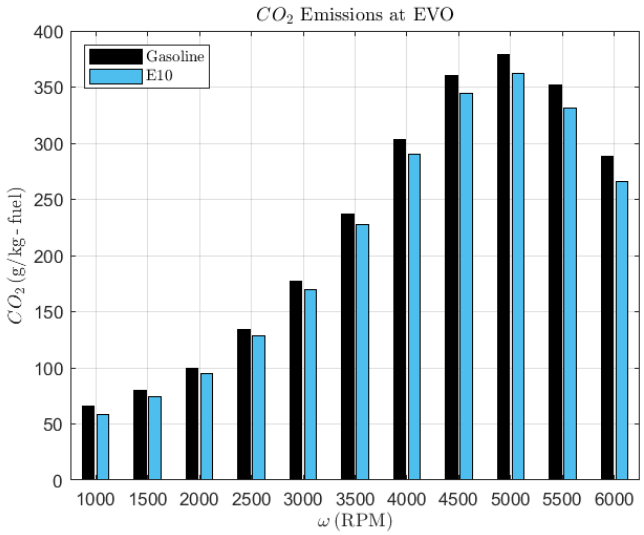

Figure 24. CO_2 emissions at EVO for gasoline and E10.

These emissions are an estimate based on the emissions of CO and because of this, they will exhibit the same behavior. Because it is an estimate, it is possible that the CO_2 emissions are not truly represented here, especially because the combustion efficiency decreases with engine speed due to the less time available to burn the fuel. Nonetheless, these emissions are lower when using E10.

The consensus regarding CO_2 emissions is not very well defined and it is difficult to establish a reason as to why these are lower or higher when using ethanol blends. Some authors agree that CO_2 increases with ethanol content and others state that it decreases. Since CO_2 emissions depend on CO emissions and these increase with more complete combustion, these will be higher than CO emissions for both fuels. Nevertheless, there are some similarities.

Wang, *et al* (2015, p. 152) found that with a torque of 20 N*m, CO_2 emissions were 39.50% lower than gasoline when using hydrous ethanol with gasoline (E10W) and that a reason for its reduction is the carbon-hydrogen ratio in the fuel. In this work, it was found

that at 20 N*m of torque (3266.4 RPM for gasoline and 3251.1 RPM for E10), E10 has a reduction in emissions of 4.9%. Rosdi *et al* (2020, p. 7) and Mohammed *et al* (2021, p. 8) point out that CO_2 emissions decrease with increasing ethanol content in the fuels. In their respective experiments, Rosdi *et al* (2020, p. 7) found the highest reduction with E30, and Mohammed *et al* (2021, p. 8) with E40. Dhande *et al* (2021, p. 304) found at 1700 RPM the lowest emissions of CO_2 with E10. At this same speed, the reduction in emissions with E10 is 5.98%

Furthermore, Ansys Forte calculates the NO and NO_2 emissions, but it also calculates an Emissions Index for Nitrogen Oxides ($EINO_x$), which is the sum of the fractions of NO and NO_2 (Ansys Forte Best Practices, 2022, p. 11). Therefore, only the $EINO_x$ results of emissions as a function of CA will be presented:

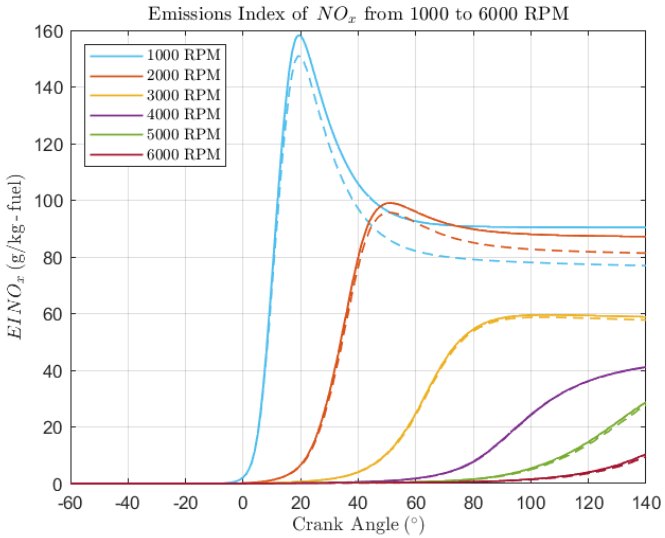

Figure 25. Emissions Index of NO_x of gasoline (–) and E10 (- - -) from 1000 to 6000 RPM.

The $EINO_x$ curves show a very different behavior than the CO and CO_2 emissions curves from 1000 to 4000 RPM. Here, unlike the other emissions curves, the $EINO_x$ curve does not lower dramatically after the peak has been reached and tends to flatten much earlier.

This is because nitrogen oxide formation is very dependent on the temperatures in the cylinder during and after combustion. The biggest differences in peak emissions are observed between 1000 and 2000 RPM and from 2000 to 3000 RPM, and from 3000 to 6000 RPM there is no longer a peak in emissions. The reduction in peak emissions for the $EINO_x$ for E10 against gasoline was 4.67%, 8.30%, and 3.38% at 1000, 1500, and 2000 RPM respectively.

From 5000 to 6000 RPM the $EINO_x$ shows a similar behavior to the CO and CO_2 emissions at the same speed range. From 3000 to 6000 RPM the differences in $EINO_x$ emissions are also considerable, but there is no longer a peak. Instead, the curve continues to increase. However, when comparing the $EINO_x$ emissions among the different speed ranges, it can be seen that the curve tends to decrease. There are no longer peaks in the higher speed range and what is even more noticeable, is that these emissions decrease as engine speed increases. In the case of the $EINO_x$, these exhibit an opposite behavior to CO emissions as will be seen in the figure below:

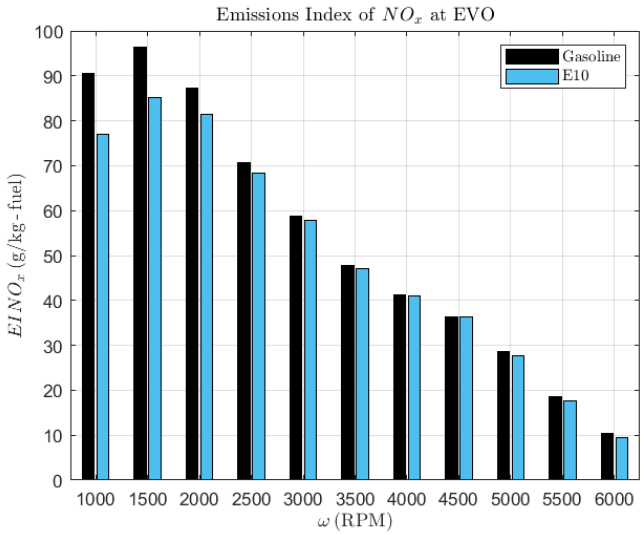

Figure 26. $EINO_x$ emissions at EVO for gasoline and E10.

Opposed to what the majority of authors report from their experiments, NO_x emissions in this work were lower with E10. However, there were some similarities. The first one is Tibaquirá *et al* (2018, p. 11), who claim that NO_x emissions are lower with ethanol blends because of the higher heat of vaporization. Likewise, Rosdi *et al* (2020, p. 6) found a NO_x emission reduction of almost 500 ppm with E10 compared to gasoline.

On the contrary, Dhande *et al* (2021, p. 304) claim higher emissions as ethanol content increases but decreases with engine speed, nonetheless, their biggest reduction in NO_x emissions was at 1700 RPM, with E10 having 30% fewer emissions than gasoline. In this work, the biggest reduction was found at 1000 RPM, with E10 producing 14.91% less emissions than gasoline. The smallest reduction in emissions was seen at 4500 RPM, with E10 having 0.11% less emissions than gasoline. The average reduction in the $EINO_x$ for E10 was 5.16%.

Additionally, Yusuf and Inambao (2021, p. 890) report the lowest emissions of NO_x with E10 at 2700 RPM, and Elshenawy *et al* (2023, p. 9) show that these emissions decrease

with higher ethanol content, but increase at higher engine speeds. Furthermore, there is only partial agreement with the results of Mohammed *et al* (2021, p. 8). They obtained increased NO_x emissions as engine speed increased, but lower emissions with higher ethanol content. In this work, these emissions indeed decrease with E10 but also decrease with engine speed.

A possible explanation for this is that since combustion efficiency is lower at higher engine speeds, the incomplete combustion occurring in the cylinder could potentially lead to lower cylinder temperatures, which as a consequence, lead to lower NO_x emissions. This is further verified when comparing the temperature curve at 1500 RPM, which is when the $EINO_x$ is at its highest, against 6000 RPM which is when the $EINO_x$ is at its lowest:

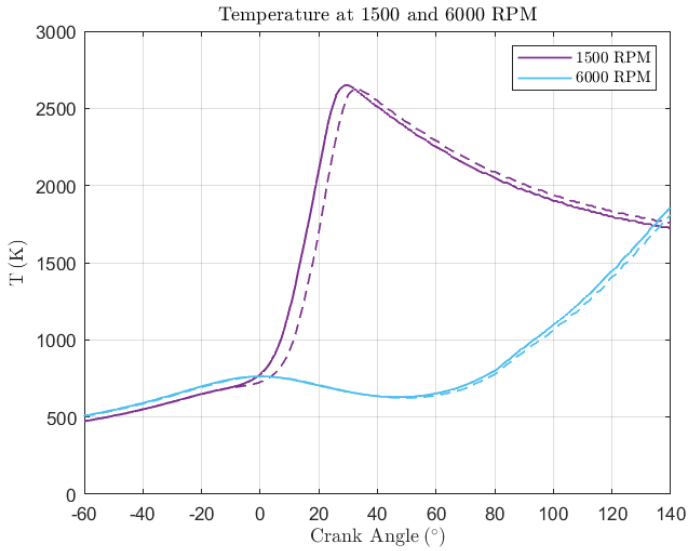

Figure 27. In-cylinder temperatures at 1500 and 6000 RPM when using gasoline (–) and E10 (- - -).

Even when the temperature at the beginning and end of the simulation is higher at 6000 RPM, the average temperature during the simulation is considerably lower compared to 1500 RPM. Here, the average temperatures were 1564.4 K and 1543.6 K for gasoline and E10, respectively at 1000 RPM, but 855.3 K and 840.5 K for gasoline and E10, respectively

at 6000 RPM. A reason for these lower temperatures could be the cooling effect produced by E10 due to its higher heat of vaporization. This increases the volumetric efficiency, as reported in the literature, and ultimately leads to lower NO_x emissions.

The unburnt hydrocarbons (UHC) plot shows an interesting behavior. Before combustion, the value is at its highest; during the simulations running pure gasoline, this value is 1000 g/kg-fuel. This value serves as a confirmation of the initial conditions, since before ignition iso-octane (gasoline's surrogate) is still premixed with the air within the cylinder and has yet to undergo combustion. In the case of E10, this amount is nearly 900 g/kg-fuel as seen in the graphs, but more precisely, the exact amount is 0.89456 kg which corresponds to the mass fraction of iso-octane present in E10. At EVO, these emissions are almost zero, at least until 3000 RPM. The following graphs show the UHC emissions for gasoline and E10 from 1000 to 6000 RPM as a function of CA:

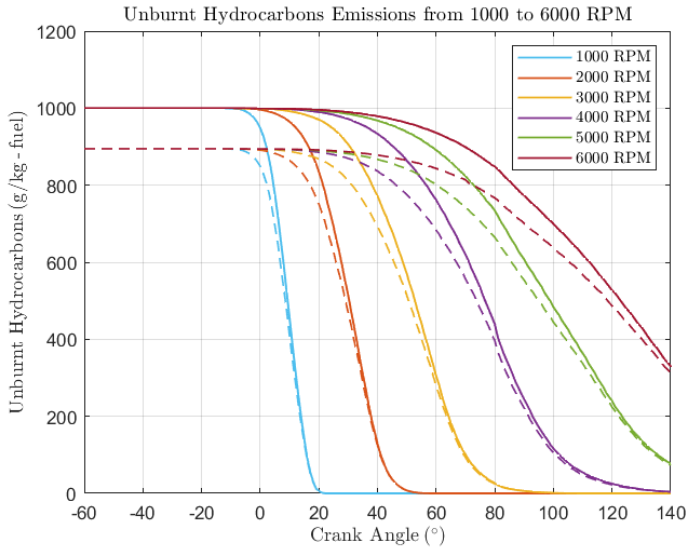

Figure 28. Unburnt Hydrocarbon emissions of gasoline (–) and E10 (- - -) from 1000 to 6000 RPM.

To have a grasp of the UHC emissions of gasoline and E10 from 1000 to 3000 RPM, the table below shows the exact values at EVO:

Table 4. Unburnt Hydrocarbon emissions of gasoline and E10 from 1000 to 3000 RPM

UHC @ EVO [g/kg - fuel]		
ω [RPM]	**Gasoline**	**E10**
1000	1.890E-11	1.322E-06
1500	2.081E-07	7.115E-06
2000	2.623E-05	2.458E-05
2500	2.309E-04	2.972E-05
3000	7.961E-03	2.890E-03

At this speed range, the difference in UHC emissions between both fuels is not consistent. At 1000 RPM, UHC emissions from E10 are 5 orders of magnitude greater than gasoline, even if the amount could be considered negligible. But from 2000 to 3000 RPM, these emissions are greater with gasoline. From what can be seen here, E10 has considerably greater emissions on average than gasoline at the lower speed range, but only because of the substantial increase in emissions at 1000 and 1500 RPM, especially at 1000 RPM.

From 2000 RPM onwards, emissions for UHC are in turn greater for gasoline than for E10 at EVO (except at 3500 RPM), two orders of magnitude greater at 4000 RPM when compared to 3500 RPM. The reason is since there is less time for combustion as engine speed increases, the combustion efficiency diminishes, meaning that the fuel mixed with air does not burn completely, leading to the emissions of this pollutant. Combustion efficiency also

diminishes because at higher RPMs the valve opening is shorter, allowing less air to enter the cylinder.

The curves from 4000 to 6000 RPM show very different behavior than the ones seen from 1000 to 3000 RPM because the UHC emissions at EVO are not near zero or negligible, but very present. Just as with the CO emissions, UHC emissions also are a product of incomplete combustion, something that happens at high engine speeds due to the shorter time for full combustion available. From 4000 to 4500 RPM, UHC emissions increase by one order of magnitude, and from 5000 to 5500 RPM emissions increase by another order of magnitude, and at 6000 RPM the order of magnitude is the same. This means that from 3500 RPM up to 5500 RPM UHC emissions increased by 4 orders of magnitude. The emissions of UHC from 1000 to 6000 RPM at EVO for gasoline and E10 are shown below:

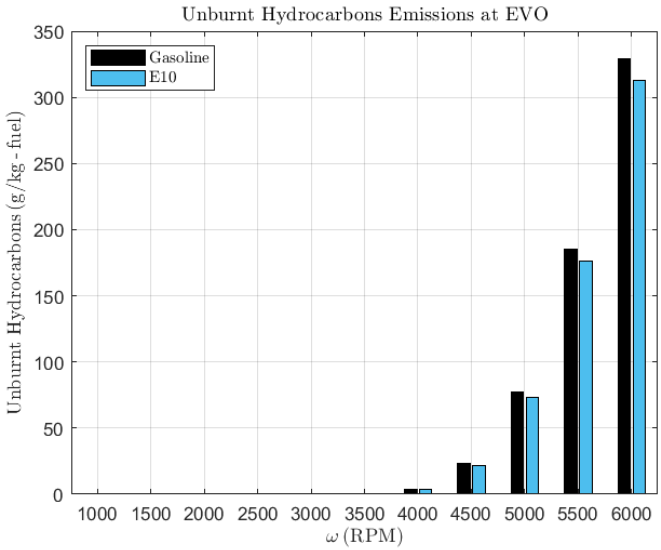

Figure 29. UHC emissions at EVO for gasoline and E10.

From Figure 29, it can be seen that from 1000 to 3500 RPM there are no bars for both fuels, hence Table 4, but from 4000 to 6000 RPM it can be seen that the smallest reduction

in emissions happens at 6000 RPM. E10 produced 5.08% less emissions at this speed than gasoline, while the biggest reduction was seen at 4500 RPM, with E10 producing 6.09% less emissions than gasoline.

On the other hand, E10 produced on average 636287.26% more UHC emissions than gasoline throughout the entire speed range, but this percentage difference is heavily affected by the results at 1000 and 1500 RPM. Despite this, the highest reduction in emissions when using E10 was at 2500 RPM with 87.12%. From 2000 to 6000 RPM, however, UHC emissions with E10 present an average reduction of 18.92%

Regarding the discussion of results, UHC emissions results demonstrate an excellent correlation with what other authors have found. Overall, all of the authors reviewed in this work agree that UHC emissions decrease with ethanol content. Pham *et al* (2015, p. 6 – 7) achieved a 25% reduction of hydrocarbon emissions (HC) when using E10 in the carbureted car, but only 3.88% compared to gasoline.

At an engine load of 20 N*m and speed of 2000 RPM, Wang *et al* (2015, p. 152) found a decrease of 40% and 44.24% in HC emissions for E10 (anhydrous ethanol) and E10W (hydrous ethanol), respectively when compared to gasoline. In this work, UHC emissions were 6.27% lower with E10 at 2000 RPM. Moreover, Yusaf *et al* (2009, p. 4) found a 24.04% reduction in HC emissions with E10 at 3000 RPM. In this work, a reduction of 63.7% of UHC emissions was found with E10 at 3000 RPM.

Also, Iliev (2021, p. 10) explains that HC decreases with greater ethanol content, something on which Dhande *et al* (2021, p. 303), Mohammed *et al* (2021, p. 8), Yusuf and

Inambao (2021, p. 891), and Hosseini *et al* (2023, p. 9) all agree on. However, despite this agreement by Hosseini *et al* (2023, p. 9), they add that HC emissions decrease with engine speed, which is contrary to what has been exposed in this work in Figure 29. Furthermore, Rosdi *et al* (2020, p. 6) report that HC emissions with ethanol blends are 6.6% lower on average than with gasoline. With higher engine speeds, complete combustion is more difficult to achieve, and therefore, UHC emissions are very high. Yet, despite this increase, E10 still has lower UHC emission values than gasoline.

Similar to the UHC, Volatile Organic Compounds (VOC) exhibit the same behavior at the same speed ranges. From 1000 to 3000 RPM, emissions become almost zero at EVO, but from 4000 to 6000 RPM, emissions are much greater at EVO. The only difference between UHC and VOC emissions is that for both gasoline and E10, VOC emissions are 1000 g/kg-fuel before ignition. The following figure shows the emissions of VOC as a function of crank angle for gasoline and E10 from 1000 to 6000 RPM:

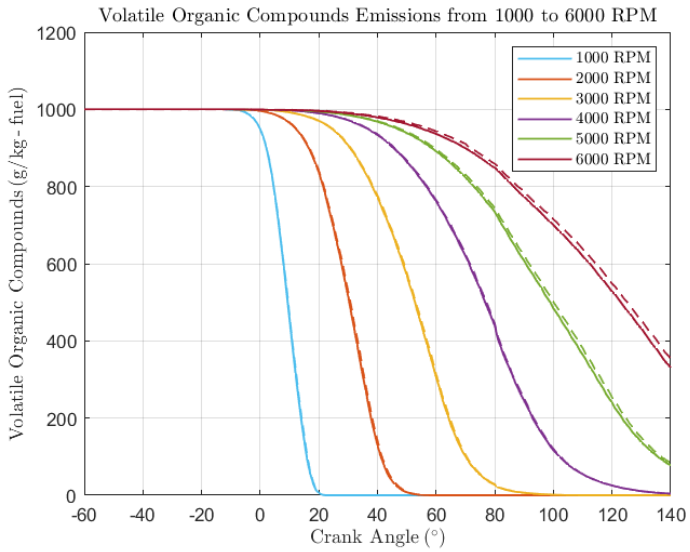

Figure 30. Volatile Organic Compounds emissions of gasoline (–) and E10 (- - -) from 1000 to 6000 RPM.

Because of these very small values of VOC, the following table shows the results of these emissions at this engine speed range:

Table 5. Volatile Organic Compounds emissions of gasoline and E10 from 1000 to 3500 RPM

VOC @ EVO [g/kg - fuel]		
ω [RPM]	**Gasoline**	**E10**
1000	2.384E-06	1.624E-02
1500	2.965E-06	3.657E-02
2000	3.039E-05	4.517E-02
2500	2.442E-04	5.261E-02
3000	8.155E-03	6.131E-02

The difference in VOC emissions between gasoline and E10 is high at this engine speed range, and even more so from 1000 to 2000 RPM. The reason is, that gasoline has many of these compounds some of which include benzene and toluene. Now, if ethanol is

added to the fuel, more of these compounds will be produced after combustion because aldehydes are produced after the oxidation of alcohols, and the aldehyde produced during the combustion of ethanol is acetaldehyde.

Nevertheless, there are some slight but important differences between the emissions of VOC for E10 and gasoline. From 3500 to 4000 RPM, VOC emissions for gasoline increase by two orders of magnitude, but for E10 it only increases by one. The increase in VOC emissions for E10 is lower between RPMs, but the emissions for E10 are considerably greater than gasoline, especially at low engine speeds. As engine speed increases, the difference between the VOC emissions of gasoline and E10 is less.

Now, the emissions of VOC from 1000 to 6000 RPM at EVO for gasoline and E10 are shown below:

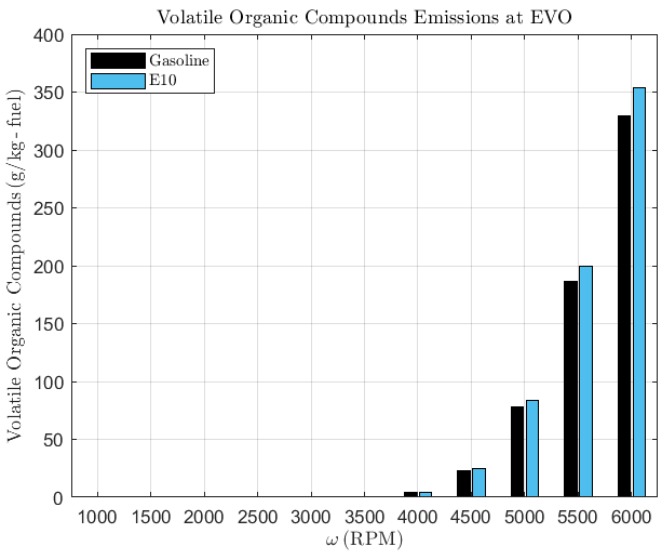

Figure 31. VOC emissions at EVO for gasoline and E10.

E10 produced on average 189570.37% more VOC emissions than gasoline throughout the entire speed range, but this percentage difference is heavily affected by the

results seen from 1000 to 3500 RPM, but especially from 1000 to 2500 RPM. This is because from 1000 to 3500 RPM, E10's VOC emissions are at least one order of magnitude higher than gasoline's. Despite this, the smallest increase in emissions when using E10 was at 4500 RPM with 6.95%. From 4000 to 6000 RPM, where the VOC emissions for both fuels have the same order of magnitude, these were 7.84% higher with E10 on average.

The greater VOC emissions found with E10 than gasoline coincide very well with González *et al.* (2018, p. 12) findings when they declare that formaldehyde and acetaldehyde emissions increase when using E10 fuel (65% in the case of acetaldehyde). In this work, the highest emissions are seen at 6000 RPM, just as with UHC emissions. Here, E10 produced 7.20% more emissions than gasoline. The problem these emissions present is their high toxicity due to their carcinogenic potential after long exposures.

One of the disadvantages of Ansys Forte is that it is not possible to know exactly which VOCs are produced. With the literature, it is only possible to have an idea of which of these may be produced. From González et al. (2018, p. 10 – 11) experiment, it can be seen that some of the VOC produced include 1,3-butadiene, benzene, formaldehyde, acetaldehyde, toluene and xylene; some of which are produced because they are found in gasoline or because they are a product of ethanol combustion.

Conclusion

By what has been presented herein, these results indicate that from a performance perspective, E10 offers a very slight deficit compared to gasoline and an important emissions reduction potential, even with higher fuel consumption. However, it is important to take into consideration, the following factors.

When simulating an internal combustion engine, there are many assumptions made to build the mathematical model, and for this reason, the results may not correlate exactly with reality. In this particular case where Ansys Forte is used, one of the limitations is that some engine conditions such as load or throttle position cannot be replicated. These conditions can only be replicated with a real engine and they influence the results obtained in terms of emissions and performance.

Other possible factors that influence the results are the simplifications made for the simulation and the lack of data available from the engine. Some simplifications include the geometries and shapes of the piston, head, and liner as well as the idealizations that were made to create these geometries. Also, not having the intake and exhaust system could have played a role in this. But the biggest simplification was the lack of a spray model, since the information related to the injector and its injection timing as well as the injected mass and duration is unknown because it is the intellectual property of the manufacturer.

However, even with these limitations, it is still possible to obtain a very good approximation of how both fuels behave in this particular type of engine. The final engine-wise related factor is the boost pressures provided by the turbocharger. Having this information for the initial conditions would certainly have given results closer to the actual performance of the engine.

Also, when it comes to results there is a partial agreement on both performance and emissions. It is partial because the results obtained with these simulations only agree with some authors, but not all of them. Ultimately, this discrepancy is often reduced to engine operating conditions, if a real engine is used, or the software and the mathematical models

employed to simulate the engine. Nevertheless, these results are reliable because of the many similarities found with the work done previously by other researchers.

In this investigation, it was possible to determine through CFD simulation the performance and emissions results of a 1.5 L turbocharged engine when fueled with gasoline and E10. The results agree with the literature and indicate that E10 offers less engine power, torque, Indicated Mean Effective Pressure, and thermal efficiency from 1000 to 6000 RPM than gasoline, but with very small to barely noticeable differences. The only considerable differences performance-wise, are found in the gross Indicated Specific Fuel Consumption (ISFC) and thermal efficiency. Due to its lower calorific value, the ISFC results with E10 were 5.45% greater on average, and the thermal efficiency was 5.08% lower on average than with gasoline at all engine speeds.

In terms of emissions, it was found that E10 produces on average, between 5 and 6%, less emissions of CO, CO_2, and $EINO_x$ throughout the entire speed range and at the Exhaust Valve Opening (EVO). But for Unburnt Hydrocarbons (UHC), these emissions are only lower than gasoline from 2000 to 6000 RPM (except 3500 RPM). Notwithstanding, the very low emissions found at engine speeds of 1000 to 3500 RPM are practically negligible. The only real concern found with E10 is the greater emissions of Volatile Organic Compounds at all speeds at EVO compared to gasoline.

Overall, from this research one can conclude that E10 could be a great starting point to solve the environmental problem, but not the best or definitive one. The reduction in emissions was so small that maybe it does not make a real difference. However, it is worth mentioning that if many vehicles used this fuel, this small reduction in emissions would be

multiplied and then an appreciable difference could be seen; at the cost of slightly higher fuel consumption and slightly lower performance. In addition, the higher VOC emissions are concerning. The health risks this poses should not be ignored and it is recommended that further studies are done regarding the use of ethanol-gasoline mixtures and their potential VOC production.

Future work on this topic may include but is not limited to, using a higher blend percentage of ethanol in the simulations to fully understand how greater ethanol content impacts emissions. Also, an attempt to correctly model the fuel spray and imitate the turbocharger conditions should be made; as well as using wall temperatures (thermal boundary conditions) that are closer to the ones obtained experimentally. But the most important one should be to validate the results obtained with this simulation using the same engine in a test bench or a chassis dynamometer with exhaust-gas analyzers because theory, or more appropriately simulation, will only take you so far.

References

Agency for Toxic Substances and Disease Registry. (August 14, 2008). *Volatile organic compounds*. Retrieved March 29, 2024 from: https://wwwn.cdc.gov/TSP/substances/ToxChemicalListing.aspx?toxid=7

Agency for Toxic Substances and Disease Registry. (March 25, 2014). *ToxFAQs™ for Nitrogen Oxides*. Retrieved February 16, 2023 from: https://wwwn.cdc.gov/TSP/ToxFAQs/ToxFAQsDetails.aspx?faqid=396&toxid=69#

Ansys Inc. (2022). *Forte Best Practices*. Retrieved March (), 2024 from: https://ansyshelp.ansys.com/account/secured?returnurl=/Views/Secured/corp/v222/en/forte_bp/forte_bp.html

Ansys Inc. (2022). *Forte Theory Manual*. Retrieved March 6, 2024, from: https://ansyshelp.ansys.com/account/secured?returnurl=/Views/Secured/corp/v222/en/forte_th/forte_th.html

Ansys Inc. (2022). *Forte Tutorials*. Retrieved March 8, 2024 from: https://ansyshelp.ansys.com/account/secured?returnurl=/Views/Secured/corp/v222/en/forte_tut/forte_tut.html

Ansys Inc. (2022). *Forte User's Guide*. Retrieved March 11, 2024 from: https://ansyshelp.ansys.com/account/secured?returnurl=/Views/Secured/corp/v222/en/forte_ug/forte_ug.html

Backhaus, R. Battery Raw Materials - Where from and Where to?. *ATZ Worldw* **123**, 8–13 (2021). https://doi.org/10.1007/s38311-021-0715-5

Beer, F., Johnston, E., Dewolf, J., Mazurek, D. (2009). *Mechanics of Materials*. United States: McGraw-Hill

Belincanta, J., Alchorne, J. A., & Teixeira Da Silva, M. (2016). The Brazilian experience with ethanol fuel: Aspects of production, use, quality and distribution logistics. *Brazilian Journal of Chemical Engineering*, *33*(4), 1091–1102. https://doi.org/10.1590/0104-6632.20160334s20150088

Binder, A., Ecker, R., Glaser, A., Müller, K. (2015). Gasoline direct injection. In: Reif, K. (eds) Gasoline Engine Management. Bosch Professional Automotive Information. Springer Vieweg, Wiesbaden. https://doi-org.udlap.idm.oclc.org/10.1007/978-3-658-03964-6_8

Borgnakke, C., Sonntag, R., (2013). *Fundamentals of Thermodynamics.* United States: John Wiley & Sons

Çengel, Y., Cimbala, J., Turner R., (2017). *Fundamentals of Thermal-Fluid Sciences.* United States: McGraw-Hill

Dhande, D. Y., Sinaga, N., & Dahe, K. B. (2021). The study of performance and emission characteristics of a spark ignition (SI) engine fueled with different blends of pomegranate ethanol. *International Journal of Energy and Environmental Engineering*, *12*(2), 295–306. https://doi.org/10.1007/s40095-020-00372-y

Dietsche, KH. (2015). Gasoline injection systems over the years. In: Reif, K. (eds) Gasoline Engine Management. Bosch Professional Automotive Information. Springer Vieweg, Wiesbaden. https://doi-org.udlap.idm.oclc.org/10.1007/978-3-658-03964-6_5

Dietsche, KH., Kuhlgatz, D. (2015). History of the automobile. In: Reif, K. (eds) Gasoline Engine Management. Bosch Professional Automotive Information. Springer Vieweg, Wiesbaden. https://doi-org.udlap.idm.oclc.org/10.1007/978-3-658-03964-6_1

Elshenawy, A. A., Razik, S. M. A., & Gad, M. S. (2023). Modeling of combustion and emissions behavior on the effect of ethanol–gasoline blends in a four stroke SI engine. Advances in Mechanical Engineering, 15(3), 16878132231157178. https://doi.org/10.1177/16878132231157178

Fédération Internationale de l'Automobile. (2022). *2022 Formula 1 Technical Regulations*. *9*, 1–180. Retrieved March 9, 2022 from: https://www.fia.com/regulation/category/110

Formula One World Championship Limited. (2021, October 5). *WATCH: How Formula 1 is striving to create a 100% sustainable fuel*. Retrieved March 10, 2022 from: https://www.formula1.com/en/latest/article.watch-how-formula-1-is-striving-to-create-a-100-sustainable-fuel.1ENHVTjKDbXNOIidEJ8okc.html

Fountain, H. (2021, August 23). Climate Change Contributed to Europe's Deadly Floods, Scientists Find. *Forbes*. Retrieved March 8, 2022 from: https://www.nytimes.com/2021/08/23/climate/germany-floods-climate-change.html

Fountain, H. (2021, November 17). Hotter Summer Days Mean More Sierra Nevada Wildfires, Study Finds. *The New York Times*. Retrieved March 8, 2022 from: https://www.nytimes.com/2021/11/17/climate/climate-change-wildfire-risk.html

Frauhammer, J., Schenck zu Schweinsberg, A., Winkler, K. (2015). Catalytic emission control. In: Reif, K. (eds) *Gasoline Engine Management*. Bosch Professional Automotive Information. Springer Vieweg, Wiesbaden. https://doi-org.udlap.idm.oclc.org/10.1007/978-3-658-03964-6_18

General Motors Corporate Newsroom. (2021, January 28). *General Motors, the Largest U.S. Automaker, Plans to be Carbon Neutral by 2040*. Retrieved March 9, 2022 from: https://media.gm.com/media/us/en/gm/home.detail.html/content/Pages/news/us/en/2021/jan/0128-carbon.html

González, U., Schifter, I., Díaz, L. *et al*. Assessment of the use of ethanol instead of MTBE as an oxygenated compound in Mexican regular gasoline: combustion behavior and emissions. *Environ Monit Assess* **190**, 700 (2018). https://doi-org.udlap.idm.oclc.org/10.1007/s10661-018-7083-7

Hoang, Anh & Tran, Quang-Vinh & Al Tawaha, Abdel Rahman & Viet, Pham & Nguyen, Xuan Phuong. (2019). Comparative analysis on performance and emission characteristics of an in-Vietnam popular 4-stroke motorcycle engine running on biogasoline and mineral gasoline. *Renewable Energy Focus*. 28. 10.1016/j.ref.2018.11.001. Retrieved on August 29, 2021

Hofmann D., Mencher B., Häming W., Hess W. (2015) Basics of the gasoline (SI) engine. In: Reif K. (eds) *Gasoline Engine Management*. Bosch Professional Automotive Information. Springer Vieweg, Wiesbaden. https://doi-org.udlap.idm.oclc.org/10.1007/978-3-658-03964-6_2

Hosseini, H., Hajialimohammadi, A., Jafari Gavzan, I., & Ali Hajimousa, M. (2023). Numerical and experimental investigation on the effect of using blended gasoline-ethanol fuel on the performance and the emissions of the bi-fuel Iranian national engine. *Fuel*, *337*, 127252. https://doi.org/10.1016/j.fuel.2022.127252

Iliev, S. (2021). A Comparison of Ethanol, Methanol, and Butanol Blending with Gasoline and Its Effect on Engine Performance and Emissions Using Engine Simulation. *Processes*, *9*(8). https://doi.org/10.3390/pr9081322

Iliev, S.P. (2015). Developing of a 1-D Combustion Model and Study of Engine Performance and Exhaust Emission Using Ethanol-Gasoline Blends. In: Yang, GC., Ao, SI., Gelman, L. (eds) Transactions on Engineering Technologies. Springer, Dordrecht. https://doi-org.udlap.idm.oclc.org/10.1007/978-94-017-9804-4_6

Jayanti, S. (2018). Introduction. In *Computational Fluid Dynamics for Engineers and Scientists* (pp. 1–16). Springer Netherlands. https://doi.org/10.1007/978-94-024-1217-8_1

Kajishima, T., & Taira, K. (2017). Numerical Simulation of Fluid Flows. In *Computational Fluid Dynamics: Incompressible Turbulent Flows* (pp. 1–22). Springer International Publishing. https://doi.org/10.1007/978-3-319-45304-0_1

Köhler, C., Allgeier, T. (2015). Exhaust emissions. In: Reif, K. (eds) *Gasoline Engine Management*. Bosch Professional Automotive Information. Springer Vieweg, Wiesbaden. https://doi-org.udlap.idm.oclc.org/10.1007/978-3-658-03964-6_17

Macmillan Encyclopedia of Energy. (n.d.). *Alternative Fuels and Vehicles*. Retrieved October 30, 2022 from: https://www.encyclopedia.com/environment/encyclopedias-almanacs-transcripts-and-maps/alternative-fuels-and-vehicles

Minnesota Department of Health. (October 20, 2022). *Volatile Organic Compounds in Your Home*. Retrieved March 29, 2024 from: https://www.web.health.state.mn.us/communities/environment/air/toxins/voc.htm

Mohamad, B., Szepesi, G. L., & Bollo, B. (2018). Review Article: Effect of Ethanol-Gasoline Fuel Blends on the Exhaust Emissions and Characteristics of SI Engines. In B. Jármai Károly and Bolló (Ed.), *Vehicle and Automotive Engineering 2* (pp. 29–41). Springer International Publishing. https://doi.org/10.1007/978-3-319-75677-6_3

Mohammed, M. K., Balla, H. H., Al-Dulaimi, Z. M. H., Kareem, Z. S., & Al-Zuhairy, M. S. (2021). Effect of ethanol-gasoline blends on SI engine performance and emissions. Case Studies in Thermal Engineering, 25, 100891. https://doi.org/10.1016/j.csite.2021.100891

National Aeronautics and Space Administration. (2022, March 9). *Overview: Weather, Global Warming and Climate Change*. Retrieved March 9, 2022 from: https://climate.nasa.gov/resources/global-warming-vs-climate-change/

Nunez, C. (2019, July 15). Biofuels, explained. *National Geographic*. Retrieved March 10, 2022 from: https://www.nationalgeographic.com/environment/article/biofuel

Office of Energy Efficiency and Renewable Energy. (n.d.). *Biofuel Basics*. Retrieved October 30, 2022 from: https://www.energy.gov/eere/bioenergy/biofuel-basics

Pham, H., Tuyen, P., Pham, M., & Le Anh, T. (2015). *Influence of E10, E15 and E20 fuels on performance and emissions of in-use gasoline passenger cars*. https://www.researchgate.net/publication/340023625_Influence_of_E10_E15_and_E20_fuels_on_performance_and_emissions_of_in-use_gasoline_passenger_cars

Phillips, N. (2020, March 4). Climate change made Australia's devastating fire season 30% more likely. *Nature*. Retrieved March 8, 2022 from: https://www.nature.com/articles/d41586-020-00627-y

Pulkrabek, W. (1997). *Engineering Fundamentals of the Internal Combustion Engine*. United States: Prentice Hall. Retrieved March 30, 2024 from: https://2k9meduettaxila.files.wordpress.com/2012/09/engineering-fundamentals-of-the-internal-combustion-engine-2k9meduettaxila-wordpress-com.pdf

Rosdi, S. M., Mamat, R., Alias, A., Hamzah, H., Sudhakar, K., & Hagos, F. Y. (2020). Performance and emission of turbocharger engine using gasoline and ethanol blends. *IOP Conference Series: Materials Science and Engineering*, *863*(1), 12034. https://doi.org/10.1088/1757-899X/863/1/012034

Royal Society (Great Britain). (2008). *Sustainable biofuels: prospects and challenges*. The Royal Society. Retrieved March 9, 2022 from: https://royalsociety.org/~/media/royal_society_content/policy/publications/2008/7980.pdf

Sinharoy, P., McAllister, S.L., Vasu, M., Gross, E.R. (2019). Environmental Aldehyde Sources and the Health Implications of Exposure. In: Ren, J., Zhang, Y., Ge, J. (eds)

Aldehyde Dehydrogenases. *Advances in Experimental Medicine and Biology, vol 1193*. Springer, Singapore. https://doi-org.udlap.idm.oclc.org/10.1007/978-981-13-6260-6_2

Stan, C. (2017). Alternative Fuels. In: Alternative Propulsion for Automobiles. Springer, Cham. https://doi-org.udlap.idm.oclc.org/10.1007/978-3-319-31930-8_3

Tibaquirá, J., Huertas, J., Ospina, S., Quirama, L., & Niño, J. (2018). The Effect of Using Ethanol-Gasoline Blends on the Mechanical, Energy and Environmental Performance of In-Use Vehicles. Energies, 11(1), 221. MDPI AG. Retrieved from http://dx.doi.org/10.3390/en11010221

Ullmann J., Allgeier T. (2015) Fuels. In: Reif K. (eds) Gasoline Engine Management. Bosch Professional Automotive Information. Springer Vieweg, Wiesbaden. https://doi-org.udlap.idm.oclc.org/10.1007/978-3-658-03964-6_3

United States Environmental Protection Agency. (2022, February 25). *Global Greenhouse Gas Emissions Data*. Retrieved March 8, 2022 from: https://www.epa.gov/ghgemissions/global-greenhouse-gas-emissions-data

Volkswagen AG. (2022). *Group strategy NEW AUTO - Mobility for Generations to Come*. Retrieved March 9, 2022 from: https://www.volkswagenag.com/en/group/strategy.html

Wang, X., Chen, Z., Ni, J., Liu, S., & Zhou, H. (2015). The effects of hydrous ethanol gasoline on combustion and emission characteristics of a port injection gasoline

engine. *Case Studies in Thermal Engineering*, *6*, 147–154. https://doi.org/10.1016/j.csite.2015.09.007

Wolber, J., Schelhas, P., Müller, U., Baumann, A., Keller, M. (2015). Fuel supply. In: Reif, K. (eds) Gasoline Engine Management. Bosch Professional Automotive Information. Springer Vieweg, Wiesbaden. https://doi-org.udlap.idm.oclc.org/10.1007/978-3-658-03964-6_6

World Health Organization. (2022). *Air pollution*. Retrieved March 8, 2022 from: https://www.who.int/health-topics/air-pollution#tab=tab_1

Yusaf, T., Buttsworth, D., & Najafi, G. (2009). Theoretical and experimental investigation of SI engine performance and exhaust emissions using ethanol-gasoline blended fuels. *ICEE 2009 - Proceeding 2009 3rd International Conference on Energy and Environment: Advancement Towards Global Sustainability*, 195–201. https://doi.org/10.1109/ICEENVIRON.2009.5398648

Yusuf, A.A., Inambao, F.L. Effect of low bioethanol fraction on emissions, performance, and combustion behavior in a modernized electronic fuel injection engine. *Biomass Conv. Bioref.* **11**, 885–893 (2021). https://doi-org.udlap.idm.oclc.org/10.1007/s13399-019-00519-w

Zareei, J., Kakaee, A.H. Study and the effects of ignition timing on gasoline engine performance and emissions. *Eur. Transp. Res. Rev.* **5**, 109–116 (2013). https://doi-org.udlap.idm.oclc.org/10.1007/s12544-013-0099-8